Geologica Acta, Vol.9, Nos 3-4, September-December 2011, 363-387
DOI: 10.1344/105.000001694
Available online at www.geologica-acta.com

Jadeitite from Guatemala: new observations and distinctions among multiple occurrences

G. E. HARLOW [1] V. B. SISSON [2] S. S. SORENSEN [3]

[1] Department of Earth and Planetary Sciences, American Museum of Natural History
New York, New York, USA. E-mail: gharlow@amnh.org

[2] Department of Earth and Atmospheric Sciences, University of Houston
Houston, TX, USA. E-mail: j_sisson@netzero.net

[3] Department of Mineral Sciences, Smithsonian Institution
Washington, DC, USA. E-mail: sorensen@si.edu

ABSTRACT

In Guatemala, jadeitite occurs as blocks in serpentinite mélange in distinct settings on opposite sides of the Motagua fault. Jadeitites north of the Motagua fault are associated with eclogites, blueschists, and garnet amphibolites and distributed over a 200km E-W area. Omphacitite, omphacite - taramite metabasite, albitite, and phengite rock are found with jadeitite. The assemblages indicate formation at 6-12kbar and 300-400°C, however jadeite - omphacite pairs yield T from ~200 to >500ºC for jadeite crystallization. Jadeitites south of the Motagua fault are sourced from three separate fault slices of serpentinite in Jalapa and Zacapa departments and are distinctive:

1) Jadeitite near Carrizal Grande is found in serpentinite with lawsonite eclogites, variably altered to blueschist, and rarely in schists. A large jadeite – omphacite gap and lawsonite suggests T=300-400°C, but at high P as indicated by the presence of quartz: P>12-20kbar. Lawsonite eclogites (P=20-25kbar, T=350-450°C) occur with these jadeitites.

2) At La Ceiba, jadeitites coexist with omphacite blueschists and contain late-stage veins of quartz, diopside, cymrite, actinolite, titanite and vesuvianite. A large jadeite – omphacite gap suggests 300-400°C, but at lower P as indicated by quartz + albite: P=10-14kbar.

3) At La Ensenada jade i tites occur with lawsonite-glaucophane blueschists and chloritite. It is a fine-grained jadeite-pumpellyite rock, intensely deformed and veined with grossular, omphacite, albite and titanite, but no quartz. A large jadeite–omphacite gap and pumpellyite suggest ~200-~300°C at lower P consistent with primary albite: P=6-9kbar. The silicates contain little iron.

KEYWORDS | Jadeitite. Serpentinite. Mélange. HP–LT rock. Subduction processes.

INTRODUCTION

The jade of the indigenous Middle American cultures of Mexico and Central America is jadeite rock (jadeitite) as well as the material from which jadeite derived its name (Foshag, 1957; Harlow et al., 2007). After knowledge of the sources was lost to the original inhabitants of Middle America, it was not until the early 1950s that workshop materials were discovered by Foshag and Leslie (1955) and then boulders by McBirney et al. (1967). These led to the eventual recognition that jadeitite was hosted in serpentinite mélanges north of the Río Motagua in central Guatemala (e.g., Hammond et al., 1979; Harlow, 1994). The river generally follows the Motagua fault zone (this zone includes many nearby parallel and sub-parallel faults within the valley), the broad boundary between the North American and Caribbean plates. The location (north versus south) is best referenced to the active strand in the Motagua fault zone, the Motagua fault, which has other names locally, such as the Cabañas fault in the central part of the valley, named for the town closest to the epicenter of the 1976 earthquake. The jadeitite-bearing region was demarked as extending between Río La Palmilla and the town of Estancia de La Virgen, a distance of about 14km (Fig. 1) and was the only described jadeitite source in Central America prior to the year 2000. A resurgence of interest and scientific recognition of a much larger areal distribution awaited the serendipitous recognition by Russell Seitz, an investigator from a 1970s jade sourcing project, of a single piece of jade (jadeitite) at a shop in Antigua Guatemala that closely resembled blue-green Olmec jade (Seitz et al., 2001; Taube et al., 2004). This discovery combined with severe flooding caused by Hurricane Mitch in 1998, which turned over the boulder fields in drainages south of the Río Motagua, led to a resurgence of interest in jadeitite sources by the authors and others. Over a few years we were shown previously undescribed sources by Guatemalan geologists and local jade hunters (jaderos), including ones traversed by Río El Tambor (Río Jalapa in Jalapa Department) and its tributaries, south of Río Motagua. In addition to the jadeitite, largely overlooked eclogite occurrences were encountered which increased the interest and potential scientific significance among the serpentinite-hosted high-pressure/low-temperature (HP–LT) rocks of the Motagua fault zone. Commercial and artisanal exploration for jade and our own field studies over the intervening years have revealed that sources north of the fault are distributed sporadically in serpentinite over at least 110km E-W and a smaller distribution of sources of 3 distinct clusters of jadeitite sources, within 11km of one another. Most recently we sampled an area of jadeitites near Rosario, east of Lago Izabal, and 203km from Saltán the most western source. Although we have mentioned some of these new sources in part in other papers (Seitz

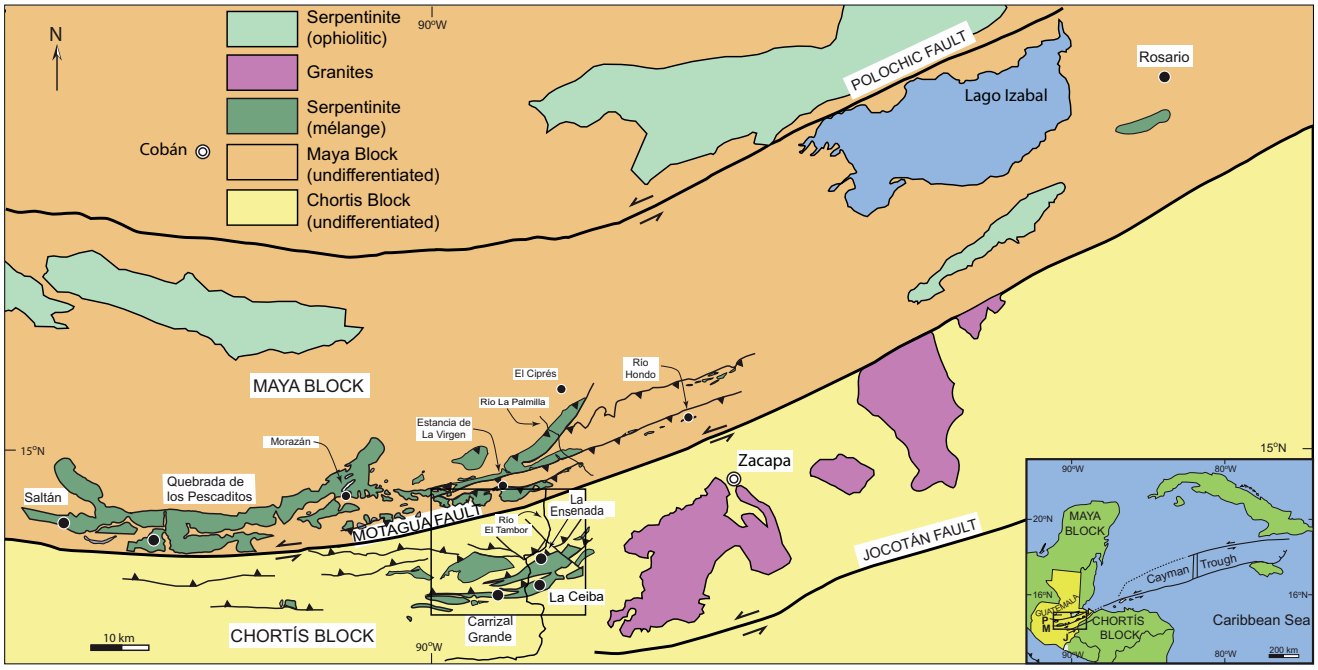

FIGURE 1 | **Regional map showing the location of jadeitite occurrences along the Motagua Valley of central Guatemala. Serpentinite bodies are differentiated between lizardite-dominant thrust blocks (ophiolitic) and antigorite-dominant HP–LT mélange. Late Cretaceous – Early Tertiary granite bodies in the Chortís block are shown with hachures. The area in Fig. 3 is defined by the outlined rectangle in lower portion of the figure. M: Motagua fault, P: Polochic fault and J: Jocotan Fault.**

et al., 2001; Harlow et al., 2004a, 2006a, 2007), here we describe these jadeitites and jade-like rocks to point out their location-distinctive appearance, mineralogy, and microtextures and inferences for origin among the HP–LT blocks in the serpentinite mélanges straddling the Motagua fault zone in Guatemala.

GEOLOGICAL SETTING

The boundary between the North American and Caribbean plates in Guatemala is defined by the Motagua fault zone, one of three left-lateral, subparallel strike-slip fault systems: Polochic (Polochic–Chixoy), Motagua, and Jocotán (Jocotán–Chamelecón); (see Fig. 1). Tectonic slices of serpentinite mélange containing HP–LT rocks occur adjacent to the Motagua fault, both north (regionally the Maya block) and south (Chortís block). These blocks are distinctly different as the basement of the Chortís block contains a significant mafic component, while the Chuacús Series of the Maya block is dominantly quartzofeldspathic. Lithologies on either side of the Motagua fault, with the exception of the serpentinites and related rocks, are completely different from each other (Francis, 2005; Alvarado et al., 2007; Martens et al., 2007a; Francis et al., in preparation), suggesting simple juxtaposition of differing terranes and/or considerable displacement along the Motagua fault. The units in the Maya block to the north include the high-metamorphic-grade Chuacús Complex (McBirney, 1963; van den Boom, 1972; Ortega-Gutiérrez et al., 2004; Martens et al., 2007b), Paleozoic sediments of the Santa Rosa Group and deformed granites. The Chortís block south of the fault contains the greenschist facies San Diego phyllite, the amphibolites facies Las Ovejas complex with felsic and mafic intrusives, and large, relatively undeformed granitoids of uncertain age. There are several granitic intrusions in the Chortís block that are of Late Cretaceous and Early Tertiary age (Donnelly et al., 1990). The block also contains the El Tambor ophiolite complex, recently dated on the basis of radiolaria to be of Late Jurassic age (Chiari et al., 2006). Both blocks are mantled with modern arc volcanics to the south and west, further complicating interpretation.

Until recently, the HP–LT belts along the Motagua fault had been assigned to a single tectonic (collisional) event in the Late Cretaceous, although all studies noted the strong lithotectonic dichotomy in these terranes (see Donnelly et al., 1990). North of the Motagua fault, serpentinite mélange hosts garnet amphibolite, omphacite-taramite metabasite, jadeitite, albitite, and, more recently reported, altered clinozoisite - amphibole - eclogite in the western reaches of the serpentinite mélange (Tsujimori et al., 2004a; Brueckner et al., 2005). These rocks span a wide range of conditions, from greenschist - blueschist at lower P (200-400°C at ≤1GPa) to moderate low-temperature eclogite facies of 500-600°C at ~2GPa. In contrast, south of the fault, assemblages include lawsonite eclogite, blueschist, and jadeitite in serpentinite matrix that record peak P-T conditions among the coldest and wettest deep subduction trajectories on Earth, to ~2.6GPa and only ~470ºC (Tsujimori et al., 2006a, b). Compounding the differences, Harlow et al. (2004a) reported disparate $^{40}Ar/^{39}Ar$ ages on the mica and amphibole from these HP–LT rocks: north of the fault ages range between 77 and 65Ma, whereas rocks south of the fault yield ages of 125-116Ma. Subsequent determinations of five Sm-Nd mineral isochrons from eclogites both north and south of the fault have yielded ages of 144-126Ma (Brueckner et al., 2009). The rarely recorded presence of jadeitite, lawsonite eclogite and a tectonic-timing conundrum represent only a small aspect of the complex geology exposed in central Guatemala related to the boundary region between the Maya and Chortís blocks, let alone the North American and Caribbean plates.

JADEITITE: OCCURRENCE AND ASSOCIATIONS

The jadeitite found north of the Motagua fault was described by Harlow (1994), so the intent here is to present new observations and interpretations, while only summarizing the generalizations in that paper. Moreover, as jadeitite from south of the Motagua fault has not been described in detail and is distinctly different from jadeitite found north of the Motagua fault, a greater portion of the attention is devoted to these. Fundamentally, most of the jadeitite occurrences were discovered by jade hunters (jaderos in Spanish) who have shown them to us. This transfer of information has resulted in the considerable growth in areal distribution presented here. The rocks studied and abbreviations for mineral names are given in Table I, Electronic Appendix, available in www.geologica-acta.com

The jadeitite occurrences along the Motagua fault zone are all sourced within serpentinite-dominant mélange (that is mélange in which serpentinite dominates both as matrix and as broken up blocks–an abundance of mixed sedimentary and HP–LT rocks is not observed). The serpentinites consist predominantly of antigorite, with lesser lizardite (no chrysotile has been observed) with interstitial magnetite, magnesite, chlorite, talc, pentlandite and low-T Ni-sulfides and occasional relict clinopyroxene, pseudomorphed orthopyroxene (bastite) or magnesiochromite (Harlow et al., 2006b; Bertrand and Vuagnat, 1976, 1980). There are subtle differences in the mineralogy of the serpentinite, as a whole, from the north to the south sides of the Motagua fault, particularly in the relative abundance of magnesite and talc, but otherwise the recorded gross differences are not large (Harlow et al., 2006b). The protolith has so far

been interpreted as dominantly harzburgite but probably ranges from dunite with rare podiform chromite through harzburgite to spinel lherzolite (Bertrand and Vuagnat, 1976, 1980; Harlow et al., 2006b); however, further analysis is required. Serpentinization in most samples is complete (no protolithic mineral or textural relics remain) with petrofabrics varying greatly between antigorite fels to highly sheared serpentine schists. Rare ultramafic relic phases include aluminous augite, chromite and pentlandite (Harlow et al., 2006b, 2010). All features are consistent with serpentinite produced at depth, presumably adjacent to a subduction channel responsible for the HP–LT blocks.

Irrespective of location relative to the Motagua fault, jadeitite occurs in small areas, typically extending no more than a few hundred meters, commonly distributed as boulders and cobbles of a dismembered larger body sitting on (and in) serpentinite (Fig. 2). Even more commonly the jadeitite occupies drainages cutting through or downstream from the serpentinite mélange. In some cases these broken blocks are dispersed with other HP–LT lithologies along alignments, which we interpret as faults within the mélanges, or in slumped fields in serpentinite downhill from such a boundary. Boulders can measure up to 5meters across (e.g., at Quebrada Seca, about 2.5km SE of Carrizal Grande, south of the Motagua fault, or in Río La Palmilla, north of the Motagua fault) although meter or smaller sizes are most common. Jadeitite rarely occurs as discrete blocks or veins with contact relationships to serpentinite. Jadeitite blocks in place (although probably with tectonic contacts) are limited to La Ceiba (S), Quebrada Seca, near Carrizal Grande (S) and El Ciprés in the Sierra de las Minas (N) (see Figs. 1 and 3), although the latter has been dismembered by jade extraction (Sorensen et al., 2005, 2010).

Occurrences North of the Motagua fault

Fields of jadeitite generally occur in what appear to be distinct fault segments or along boundaries between serpentinite and Chuacús Series basement. The distribution now extends from the westernmost occurrence, just south of the town of Saltán, Baja Verapaz department (14.9005°N, 90.5983°W), to the town of Río Hondo, Zacapa department (15.0444ºN 89.5853W), spanning a distance of 110km (Fig. 1). The newly-visited far-eastern source area is near Rosario, Izabal department (15.6866N, 88.8998W), more than 200km from Saltán. The jadeitites share many characteristics and occur with a limited assemblage of other HP–LT rocks. Most of the jadeitite is massive and whitish to pale gray or pale green (Fig. 4A) and commonly with transecting veins of coarser jadeitite or albitite-like alteration. Blocks of white-to-mauve jadeitite (Fig. 4B) have been found in a *quebrada* (dry gulch) near Saltán, the western extent to date, and have a distinctive phase assemblage as well as appearance. Mostly medium green jadeitite has been recovered from near Rosario at the eastern limit of occurrences, and this material is not distinctive in terms of phase assemblage compared to the bulk of jadeitite north of the Motagua fault. The jadeitite blocks show cataclastic to sheared textures in addition to the veins. Albitization around block margins and fractures post-dating jadeite-veining is common; complete replacement of jadeitite by albitite typically occurs toward the boundary of a block with serpentinite host, if contact relationships can be observed. The jadeitite - serpentinite contact zone consists of concentrically foliated blackwall mineralogy (actinolite + clinochlore ± talc) a few centimeters to perhaps a meter thick, penetrated by centimeter to decimeter wide bundles of acicular actinolite aligned radial to the block. Sorensen et al. (2010) have described a complete contact assemblage at El Ciprés, documenting not only the transition from jadeitite to albitite to altered ultramafic boundary to serpentinite but also the chemical transport between and through each zone. Rocks that have the same massive appearance as jadeitite but are darker green tend to be dominated by omphacite and thus are actually omphacitites. There is an intimate association of jadeitite and albitite north of the Motagua fault, which is in part due to the alteration of jadeitite to albitite, but albitite occurs as a distinct rock without apparent replacement texture (Harlow, 1994). In addition, albite-phengite rocks, phengite rocks (noticeably dense from high Ba content; Harlow, 1995), taramite-omphacite metabasite (Harlow and Donnelly, 1989), omphacitite, and garnet-clinozoisite amphibolite or clinozoisite eclogite are commonly associated with the jadeitites. Garnet amphibolite is found only in the eastern extent (as far west as Morazán) and eclogite in the west (as far east as

FIGURE 2 | **Broken jadeitite blocks sitting on serpentinite subsurface, Piedra Parada Dos Ríos, El Cimiento Quad. (9.4km NNW of the mouth of Río La Palmilla, 300m from that river). The accumulation of smaller boulders at the bases of trees were placed there by jaderos.**

Quebrada de los Pescaditos). Omphacite inclusions in garnet of garnet amphibolite indicate that some of this lithology is retrograded eclogite. Jadeitite from north of the Motagua fault is also distinctive in its mineralogy (below).

Occurrences South of the Motagua fault

Jadeitite has probably been known in this area for a considerable time by some *jaderos* and jade workshops in Antigua, Guatemala; however, study did not commence until our first visit in 2001. There are three distinct areas in the mountains of Jalapa and Zacapa departments with very small areal distributions, typically of one to several kilometers. They are near the towns of Carrizal Grande, La Ceiba, and La Ensenada (Figs. 1 and 3) and are all within 11km of one another.

In the Carrizal Grande area, further south, jadeitite occurs mostly as isolated blocks with ill-defined contacts to adjacent serpentinite or in the drainages of several *quebradas*. Up-slope and up-stream limits appear to align with minor fault traces cutting subparallel to the overall serpentinite fault boundary (see Fig. 3). Jadeitite is generally massive and often contains conspicuous phengitic muscovite (Ms) or lawsonite phenoblasts. Color is light to medium to medium dark green with occasional dark blue-green veins colored by blue omphacite (Fig. 4C; Harlow et al., 2004b). Coexisting lithologies include lawsonite eclogite, blueschist - altered eclogite, lawsonitite, glaucophane - omphacite rock, garnet - quartz - phengite schist, and graphite - bearing quartz - mica schist (Tsujimori et al., 2006a). Near La Ceiba the jadeitite is tightly confined to a 100 meter wide exposure in serpentinite (no contacts exposed) as blocks to a few meters in size. Smaller blocks litter a *quebrada* below this exposure. The jadeitite is generally medium to dark green, on occasion intensely green, and fine-grained to microcrystalline but highly fractured (Fig. 4D). In rare cases jadeitite blocks are encapsulated by a diopside-rich rock. Coexisting tectonic blocks in the area are omphacite -

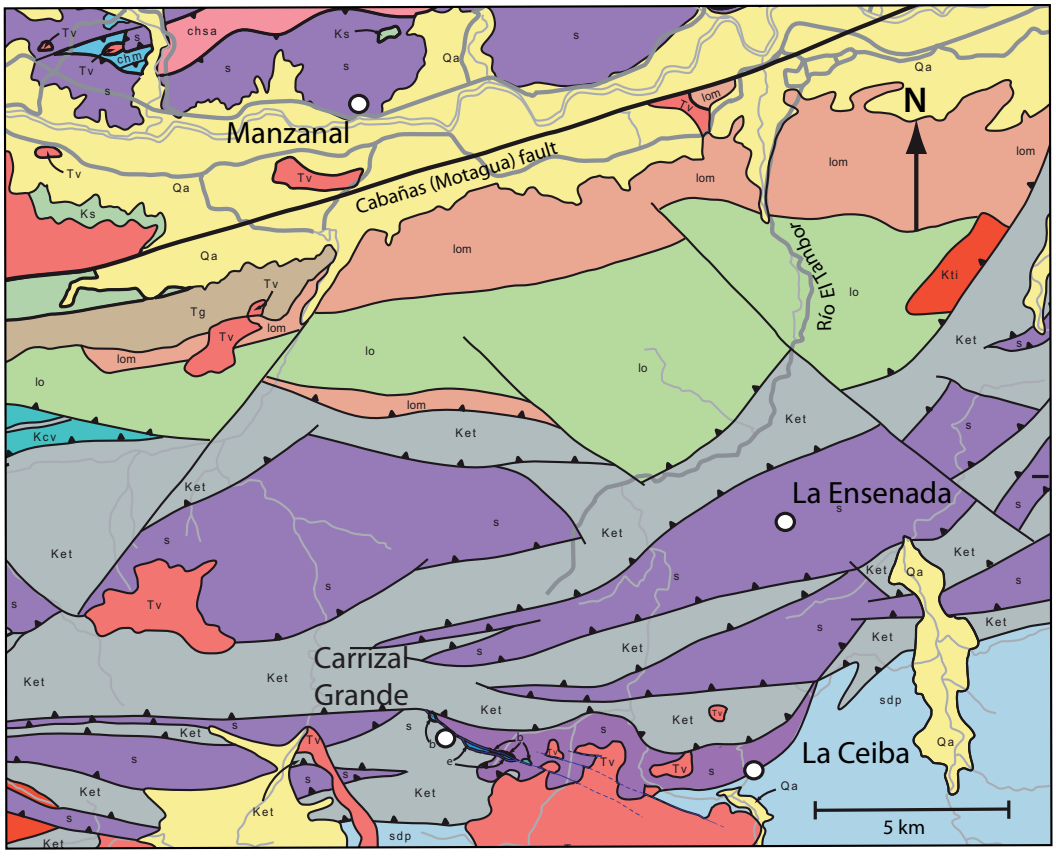

FIGURE 3 | **Geological map of area of HP–LT sources south of the Motagua fault, showing the general location of Carrizal Grande, La Ceiba, and La Ensenada; Manzanal, the first-described location north of the Motagua fault (Cabañas fault) is also shown. See the box in Fig. 1 for the location of this map. The base map is derived from a revision of an unpublished map by T. Donnelly and coworkers (Francis et al., in preparation). Formation abbreviations: chm: Chuacús marble; chsa: San Agustín formation; Kcv: Mylonitized limestone (Cerro La Virgen formation, LS tectonites); Ket: El Tambor fm.; Ks: Subinal fm.; Kti: granite plutons; lo: Las Ovejas fm. (undifferentiated); lom: Las Ovejas marble; Qa: Quaternary alluvium; s: Serpentinite; Tg: Guastatoya Fm., including mélange lithologies in most cases, but m: mélange, e: eclogite and b: blueschist shown near Carrizal Grande; sdp: San Diego phyllite; Tv: Tertiary volcanics.**

FIGURE 4 | **Photographs of jadeitite hand-samples: A) Slab of whitish coarse-grained jadeitite: MVE04-44-2, Quebrada de los Pescaditos, 2.3cm wide; B) Slab of lavender jadeitite with pumpellyite at rim: MVE07B-19-1, near Saltán, 3cm across; C) Polished slice of jadeitite w/ large phengite grains and veins of blue-green omphacite: VM02-1, Quebrada Seca, Carrizal Grande, 15cm across; D) Polished jadeitite showing mottled dark green body cut by fractures and veins of cymrite and vesuvianite + cymrite: MVE02-17-5, La Ceiba, 3cm across; E) Sawn block of pumpellyite-jadeitite cut by a vein of brown chloritite: MVE03-76-4, Quebrada La Peña, La Ensenada, sawn surface is 20cm across; F) Slab of white-green medium-grained jadeitite with zones of translucent blue-greenish microcrystalline texture: MVJ84-10-1, Manzanal, ~14cm across.**

glaucophane blueschist and epidote - amphibolite. Finally, near La Ensenada in a serpentinite slice further north, in and around an E-W trending *quebrada* are dismembered blocks (≤3m across) of a whitish gray jadeitite with green, blue, orange (grossular), and mauve streaks and spots that is a fine-grained jadeite-pumpellyite rock (this material has been sold as *jade lila* or "rainbow jade"). It occurs interlayered with a pale brown chloritite (Fig. 4E), and the associated lithologies are lawsonite blueschist and a partially amphibolitized - chloritized serpentinite. A single other occurrence of this material is found ~3km east and appears to be in the same fault slice of serpentinite.

JADEITITE: TEXTURE AND MINERALOGY

Analytical techniques

Optical and SEM/BSE petrographic and microprobe analysis of thin sections and X-ray diffraction of mineral grains were performed in this study. Electron-microprobe analysis of minerals in thin section to determine concentrations of the major constituent elements (except O) was carried out using a Cameca SX-100 microprobe at the American Museum of Natural History operated at 15kV, 10nA sample current for Na-bearing or hydrous silicates and 20kV, 15nA for oxides and sulfides, a point beam was used in all cases. Standards included natural minerals and synthetic compounds. The PAP correction scheme according to Pouchou and Pichoir (1991) was employed. Potential interferences between Ba (Lα) and Ti (Kα) were minimized by measuring X-ray counts on a PET crystal and background measured outside the window of both peaks; as long as concentrations are below ~2 wt% of either, there are no overlaps that exceed the detection limit. For all elements the detection limits are <0.01wt% but values are presented here as measured. Examination of amphiboles and micas found no detectable F or Cl, so these elements were not analyzed. No post-processing correction was made for the effect of inferred H_2O content. Estimates of Fe^{2+} and Fe^{3+} were made using an algorithm similar in concept to that of Finger (1972) to calculate Fe^{3+} from total Fe in which cation charge must sum as close as possible to twice the number of oxygen atoms plus the number of univalent anions (e.g., 6 oxygen in pyroxene), with a maximum permissible sum of cations determined by the crystal's stoichiometry (e.g., four for pyroxene as above; vacancies in large cation sites are permissible–see Harlow et al., 2006a for more details). Particularly in the case of iron-rich amphiboles, ferric-ferrous determination by the above technique may lead to poor, particularly somewhat low, totals for the C cations. Typically these totals can be improved by readjusting the FeO-Fe_2O_3 balance; but that has not been done here because the deficiencies are relatively small.

Back-scattered electron (BSE) imaging was carried out on the microprobe and on a Hitachi S-4700 Field Emission Scanning Electron Microscope (SEM). Both microprobe and SEM were equipped with either PGT-Imix (prior to April 2007) or Bruker Quantax energy-dispersive X-ray spectrometric (EDS) analyzers. X-ray diffraction identification was carried out on some powdered samples of jade using a Bragg-Brentano diffractometer or on sub-millimeter fragments and sub-millimeter areas on rock surfaces using a Rigaku DMAX/Rapid microdiffraction system employing a 100μm monocapillary collimator and monochromatized Cu Kα radiation. Patterns were interpreted with Jade 7.0 (MDI) software; although Fe fluorescence degraded the patterns in some cases, the peaks were more than sufficient for assignment of *d* values and phase identification.

Jadeite texture and mineralogy North of the Motagua fault

The macrotextures (hand samples) are generally granoblastic (grain size from 1mm to 1cm) made conspicuous in almost monomineralic masses by cleavage in blocky grains of jadeite. Weathering greatly enhances visual aspects of texture and can accentuate areas of albite and/or analcime from some combination of enhanced solubility and reduced hardness. Increased whiteness (light scattering) is common in the cores of grains or in grain clusters with grain rims more likely to be semitranslucent and greener. Although coarse grain size is typical, microcrystalline zones (Fig. 4F) and whole blocks are also found. Coarse-grained jadeitite is typically opaque while fine-grained material is more translucent. Shearing and brecciation is common, with cementation by both jadeitite and albitite assemblages (Harlow, 1994). Veins are common but not always conspicuous because of the near-monomineralic composition and lack of obvious variance in color and texture. However, very coarsely crystallized veins of jadeite exist, with walls dominated by jadeite (crystals to ~20cm) and central or interstitial white mica and/or green omphacite or late-stage alteration infilling (albitite-like), which can be decorated by black sprays of amphibole or green fingers or zones of omphacite.

Microscopic textures are highly variable, but certain features can be considered typical. Clusters of both solid and 2-phase fluid inclusions are common in the cores of jadeite grains that have survived deformational comminution. Omphacite, albite, paragonite and titanite are the most common core mineral inclusions. Moreover, in many coarse-grained jadeitites interiors of jadeite grains are dense with somewhat large solid, both mono-phase and polyphase inclusions, typically albite, analcime, paragonite, and omphacite (Fig. 5A), commonly connected

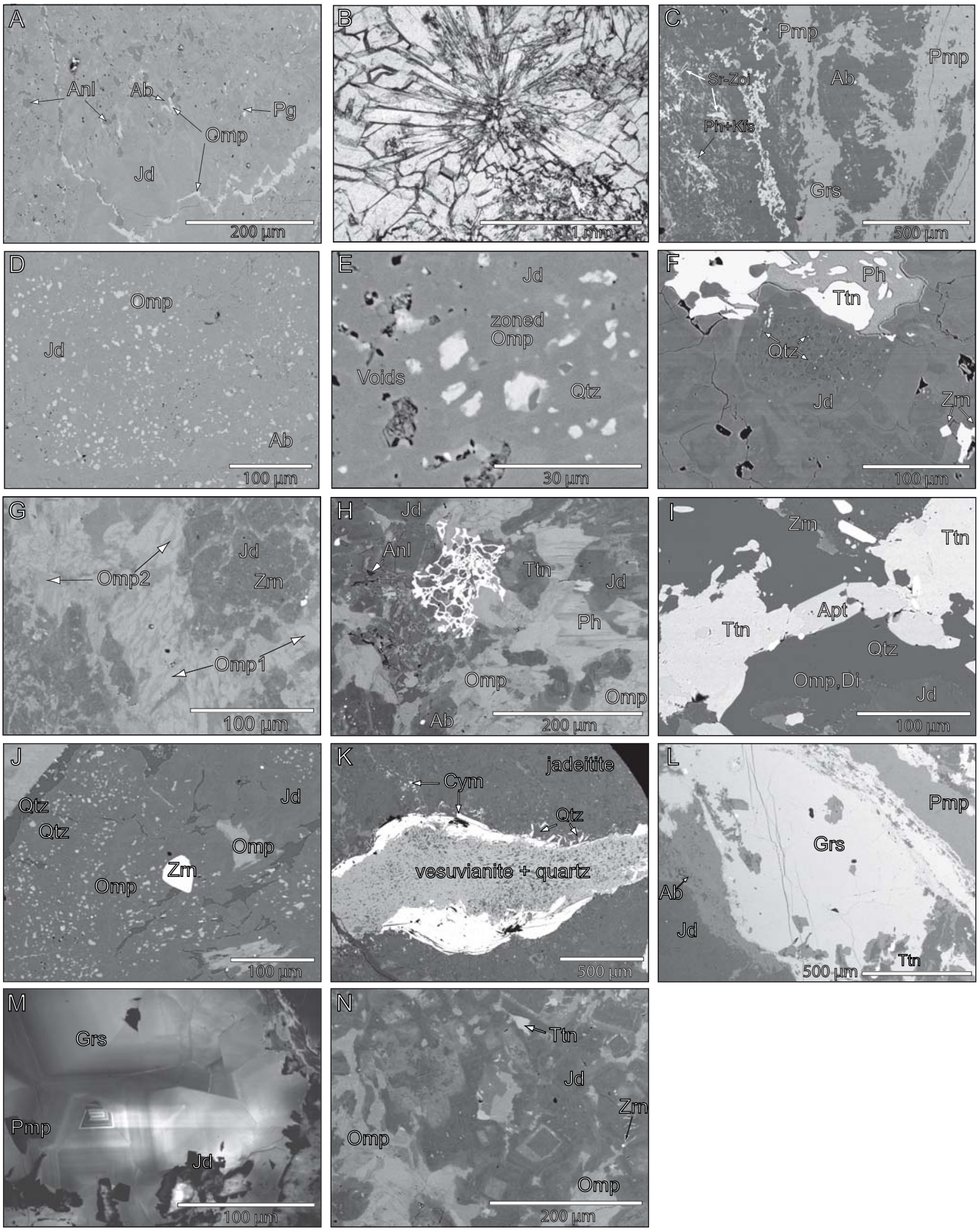
A
Anl
Ab
Pg
Omp
Jd
200 µm
B
1 mm
C
Pmp
Pmp
Sr-Zoi
Ab
Ph+Kfs
Grs
500 µm
D
Omp
Jd
Ab
100 µm
E
Jd
zoned
Omp
Voids
Qtz
30 µm
F
Ph
Ttn
Qtz
Jd
Zrn
100 µm
G
Jd
Omp2
Zrn
Omp1
100 µm
H
Jd
Anl
Ttn
Jd
Ph
Omp
Omp
Ab
200 µm
I
Zrn
Ttn
Apt
Ttn
Qtz
Omp,Di
Jd
100 µm
J
Jd
Qtz
Qtz
Omp
Zrn
Omp
100 µm
K
jadeitite
Cym
Qtz
vesuvianite + quartz
500 µm
L
Pmp
Grs
Ab
Jd
500 µm
Ttn
M
Grs
Pmp
Jd
100 µm
N
Ttn
Jd
Zrn
Omp
Omp
200 µm

by cleavage cracks. These solid inclusions commonly have associated fluid inclusions voids observed in surfaces by SEM/BSE as well as resolvable two-phase fluid inclusions via optical microscopy. These "lake district" interiors of jadeite grains typically have irregular compositional zoning and are commonly surrounded by a cleaner overgrowth of rhythmically zoned jadeite before encountering grain boundaries. Narrow boundaries between jadeite grains typically contain analcime, albite, analcime + albite or least commonly albite + nepheline; these latter two are typically in symplectitic intergrowths (Harlow, 1994). Smaller omphacite, zoisite (clinozoisite), titanite, paragonite or amphibole grains can be included in the granular boundary zone intergrowths. While not as common as the granoblastic or sheared textures, mesh and felted textures of submillimeter prismatic jadeite are found, and a few localities yield conspicuous fan-spheroidal clusters of elongate jadeite prisms relatively free of anything but two-phase fluid inclusions (Fig. 5B). In retrogressed jadeitites, inter-jadeite grain zones resemble albitite with pseudormorphing of jadeite by intergrowths of albite + omphacite ± amphibole, paragonite, preiswerkite, apatite, zoisite, titanite, banalsite, graphite, etc. (see Harlow, 1994). Sorensen et al. (2006) has shown via cathodoluminescence imaging that deformation textures plus consistent jadeite overgrowth along fracture veins are common to most jadeitite, worldwide, including those from north of the Motagua fault.

Mineralogy of samples from the originally described areas was presented in Harlow (1994); here we present mineral assemblages of samples not presented in that paper and, now, spanning the entire 200km east-west extent north of the Motagua fault (Table 1). Jadeitite exclusive of secondary veins or alteration consists fundamentally of jadeite (>90vol%, sensu stricto but more altered rocks may only be >60%) with subsidiary albite, white-to-tan mica (paragonite in most cases, with muscovite-phengite and/or phlogopite in some cases two or all three), analcime, omphacite with minor small crystals of titanite, zoisite, apatite and zircon, which all can be found as inclusions in jadeite. Rutile has only been found in one sample in the core of titanite. Veins and grain boundary alteration consist of albite + allanite or albite + nepheline, zoisite (and clinozoisite), taramitic amphibole, paragonite, phlogopite, preiswerkite, banalsite, K-feldspar, and graphite. Phengite grains can show barian overgrowths (Harlow, 1995). Zircons are generally small (<50μm long) and vary from euhedral crystals to irregular rounded ones. Their abundance correlates with K-mica abundances, and rare inclusions include holes (presumably fluid) and omphacite. As emphasized in Harlow (1994) quartz is absent from these jadeitites, not as inclusions in jadeite grains, not as a constituent phase of the rocks, nor in alterations of jadeite that retain any jadeite — jadeite + quartz is absent.

One suite of jadeitite samples north of the Motagua fault is unique for its late-stage assemblage: lavender jadeitite from near Saltán, which is the westernmost known locality (MVE07B-19). The jadeite grains form radiating prismatic clusters, although largely broken up by deformation and variably retrograded. Jadeite grains are relatively inclusion free, primarily being small (<20μm) two-phase fluid inclusions that, on occasion, have adjacent blebs of K-feldspar, and grain boundaries coated with albite ± allanite ± K-feldspar. Allanite-(Ce) with overgrowths of REE-rich clinozoisite occurs as broken prisms amidst jadeite but also with albite, so it may be either primary or an early secondary phase. Omphacite is absent and K-feldspar takes its textural place. Phengite occurs intimately with jadeite and muscovite-phengite grains are partially replaced or infiltrated by K-feldspar (variably Ba enriched) and Sr-rich zoisite-clinozoisite. Extensive albite retrogression of jadeite, which can be identified as selvages or veining through jadeite grains, contains discontinuous stringers of K-feldspar, laths of Sr-rich zoisite (sometimes overgrowing allanite), and rare crystals of pumpellyite. Isolated vesuvianite grains, graphite clusters, and boundary selvages of pumpellyite and

FIGURE 5 | **Photomicrographs: A) BSE image of jadeitite (Jd) showing cryptic-zoned grains filled with inclusions of analcime (Anl), albite (Ab), paragonite (Pg), omphacite (Omp), and now-empty fluid inclusions; rims can be relatively free of inclusions and irregular grain boundaries are decorated with the minerals found in the inclusions: MVE03-82-3, El Mapache; B) Photomicrograph (plane light, 2mm across) of radiating jadeite grains: MVE02-39-5, Pica Pica; C) BSE image of albite-pumpellyite (Pmp) selvage with grossular (Grs) stringers, Sr-zoisite (Sr-Zoi) prisms, and K-feldspar-phengite (Ph-Kfs) intergrowths on a jadeitite: MVE07B-19-1, near Saltán; D) BSE image of jadeitite showing jadeite with many blebby omphacite inclusions and a zone with more abundant fluid inclusion voids and quartz inclusions: MVE04-14-6, Quebrada Seca; E) Close-up of area with quartz (Qtz) shown in previous image; F) BSE image of jadeite grains (center) with inclusions of quartz and titanite (Ttn): MVE07-9, Carrizal Grande; G) BSE image of blue omphacite vein cutting jadeitite; jadeite exhibits cryptic zoning and overgrowth of omphacite; in vein two generations of omphacite are apparent: KT02-3, Quebrada Seca, Carrizal Grande; H) BSE image of a latticework-textured titanite typical of an association with late omphacite in jadeitite from south of the Motagua fault: JJE01-3-1, Quebrada El Silencio, Carrizal Grande; I) BSE image of titanite-apatite (Apt) intergrowth and jadeite grains surrounded by islets of omphacite plus diopside (Di) in a matrix of quartz: MVE02-15-10, Quebrada Seca, Carrizal Grande; J) BSE image of jadeite grains with small inclusions of quartz, omphacite, and fluids toward cores and small zircons (Zrn) (brightest) elsewhere and a large zircon at center: MVE02-17-5, La Ceiba; K) BSE image of a vein cutting jadeitite with quartz (dark gray) and vesuvianite (light gray) in the center and cymrite (Cym) (white) at the edges: MVE02-17-5, La Ceiba; L) BSE image of a jadeitite (dark gray) cut by vein of pumpellyite (light gray) and grossular (white): MVE04-20-1 La Ensenada; M) Cathodoluminescence (CL) image of same area as in previous image with grossular (bright), inclusions of pumpellyite (black) and jadeite (mottled bright)–subtle and sharp zoning of grossular is visible; N) BSE image of multiple stages (at least 2) of zoning from jadeite-rich-to-jadeite-poor (darker to lighter) composition of jadeite: JJE01-3-1, Quebrada El Silencio, Carrizal Grande.**

TABLE 1 | **Representative pyroxene compositions in jadeitite from north and south of the Motagua Fault**

	— NORTH —												— SOUTH —											
	West				Central				East				Carrizal Grande						La Ceiba					La Ensenada
Wt%	MVE07 B-19-4	MVE06-X-1		MVE07-1	MVE04-44-1		MVE07B-3-1		MVR07-23C		MVR07-23D		MVE04-14-6			MVE02-8-6		KT02-3	MVE02-15-6		MVE03-77-1		MVE02-15-10	MVE04-20-1	
	Jd	Jd	Omp	Aug	Jd	Omp	Jd	Omp	Jd	Omp	Jd	Omp	Jd	Jd	Omp	Jd	Omp	Omp	Jd	Omp	Jd	Omp	Di	Jd	Omp
SiO_2	59.83	59.48	56.90	54.57	59.65	56.42	57.50	59.84	59.75	56.82	59.75	56.39	59.30	58.88	54.17	59.55	57.13	56.74	58.96	56.66	57.88	54.36	55.12	58.98	56.87
TiO_2	0.07	0.08	0.30	0.69	0.03	0.03	0.05	0.05	0.10	0.05	0.04	0.08	0.03	0.03	0.14	0.02	0.15	1.86	0.08	0.11	0.26	0.05	0.14	0.47	0.09
Al_2O_3	25.30	22.47	14.12	6.89	24.31	12.26	12.38	23.83	25.21	11.98	24.18	12.24	25.13	22.17	8.34	24.48	12.03	9.81	23.67	14.01	18.69	10.06	2.54	25.31	12.84
Cr_2O_3	0.00	0.01	0.00	0.02	0.07	0.00	0.00	0.03	0.00	0.03	0.01	0.03	0.00	0.02	0.01	0.02	0.00	0.00	0.01	0.00	0.03	0.00	0.00	0.00	0.00
Fe_2O_3	0.00	0.53	3.87	9.33	0.79	4.11	2.66	0.40	0.00	1.12	0.44	5.90	0.04	0.21	9.95	0.39	2.59	1.40	0.87	1.30	3.76	5.57	1.82	0.08	0.60
FeO	0.03	1.17	1.84	0.04	0.00	0.00	0.22	0.18	0.14	2.73	0.67	10.10	0.19	1.98	6.72	0.26	0.87	2.44	0.00	0.39	1.48	3.57	4.37	0.00	0.00
MnO	0.00	0.05	0.37	0.32	0.01	0.21	0.10	0.01	0.00	0.00	0.00	0.00	0.05	0.00	0.25	0.09	0.14	0.10	0.01	0.09	0.06	0.12	0.09	0.01	0.00
MgO	0.03	1.18	5.37	8.43	0.28	7.29	8.00	0.83	0.03	7.26	0.30	3.51	0.18	0.82	2.60	0.30	7.99	8.10	0.60	7.07	1.79	6.03	12.83	0.41	9.13
CaO	0.02	1.61	7.70	12.28	0.49	10.87	11.70	1.02	0.20	12.29	0.70	2.56	0.39	2.25	9.42	0.47	11.99	11.63	0.90	10.71	3.12	12.68	20.33	0.57	12.73
BaO	0.01	0.00	0.00	0.00	0.00	0.01	0.07	0.00	0.02	0.00	0.00	0.00	0.01	0.03	0.00	0.00	0.02	0.00	0.03	0.03	0.01	0.00	0.06	0.00	0.00
Na_2O	15.40	14.20	10.06	7.47	15.39	8.91	8.46	14.80	15.23	7.89	14.96	8.93	15.06	13.82	8.89	15.04	8.16	8.12	14.75	8.85	13.09	7.41	2.72	15.17	7.79
K_2O	0.01	0.00	0.01	0.04	0.02	0.01	0.00	0.00	0.01	0.00	0.01	0.03	0.01	0.00	0.00	0.00	0.01	0.00	0.02	0.01	0.01	0.00	0.00	0.03	0.02
TOTAL	100.70	100.77	100.54	100.09	101.04	100.12	101.15	100.99	100.69	100.17	101.05	99.77	100.39	100.22	100.51	100.63	101.06	100.20	99.89	99.22	100.19	99.87	100.02	101.02	100.07
Cations per 6 O																									
Si	2.000	2.009	1.991	1.970	1.997	1.985	1.995	2.004	1.999	2.004	2.002	2.002	1.992	2.008	1.994	1.999	1.991	2.006	1.998	1.991	2.002	1.968	2.013	1.972	1.983
$^{[4]}Al$	0.000	0.000	0.009	0.030	0.003	0.015	0.005	0.000	0.001	0.000	0.000	0.000	0.008	0.000	0.005	0.000	0.009	0.000	0.002	0.009	0.000	0.032	0.000	0.028	0.017
$^{[6]}Al$	0.996	0.894	0.574	0.263	0.957	0.493	0.501	0.940	0.992	0.498	0.955	0.512	0.987	0.891	0.356	0.969	0.485	0.409	0.943	0.572	0.762	0.397	0.109	0.969	0.511
Ti	0.002	0.002	0.008	0.019	0.001	0.001	0.001	0.001	0.003	0.001	0.001	0.002	0.001	0.001	0.004	0.000	0.004	0.050	0.002	0.003	0.007	0.001	0.004	0.012	0.002
Cr	0.000	0.000	0.000	0.001	0.002	0.000	0.000	0.010	0.000	0.001	0.000	0.001	0.000	0.000	0.000	0.000	0.000	0.000	0.000	0.000	0.001	0.000	0.000	0.000	0.000
Fe^{3+}	0.000	0.014	0.102	0.254	0.020	0.109	0.070	0.005	0.000	0.030	0.011	0.094	0.001	0.005	0.276	0.010	0.068	0.037	0.022	0.035	0.098	0.152	0.050	0.002	0.016
Fe^{2+}	0.001	0.033	0.054	0.001	0.000	0.000	0.006	0.000	0.004	0.080	0.019	0.076	0.005	0.057	0.207	0.007	0.025	0.072	0.000	0.011	0.043	0.108	0.134	0.000	0.000
Mn	0.000	0.001	0.011	0.010	0.000	0.006	0.003	0.000	0.000	0.000	0.000	0.000	0.001	0.000	0.008	0.003	0.004	0.003	0.000	0.003	0.002	0.004	0.003	0.000	0.000
Mg	0.001	0.060	0.280	0.454	0.014	0.383	0.414	0.041	0.001	0.382	0.015	0.312	0.009	0.042	0.143	0.015	0.415	0.427	0.030	0.370	0.093	0.326	0.699	0.020	0.475
Ca	0.001	0.058	0.289	0.475	0.018	0.410	0.435	0.037	0.007	0.464	0.025	0.384	0.014	0.082	0.372	0.017	0.448	0.440	0.033	0.403	0.116	0.492	0.795	0.020	0.476
Ba	0.000	0.000	0.000	0.000	0.000	0.000	0.001	0.000	0.000	0.000	0.000	0.000	0.001	0.000	0.000	0.000	0.000	0.000	0.000	0.000	0.001	0.000	0.000	0.000	0.000
Na	0.998	0.929	0.682	0.523	0.999	0.608	0.569	0.961	0.988	0.540	0.972	0.615	0.981	0.914	0.635	0.979	0.551	0.557	0.969	0.603	0.877	0.520	0.193	0.983	0.527
K	0.000	0.000	0.000	0.002	0.001	0.000	0.000	0.000	0.000	0.000	0.000	0.001	0.000	0.000	0.000	0.000	0.000	0.000	0.001	0.000	0.000	0.000	0.001	0.001	0.001
Sum	4.000	4.000	4.000	4.000	4.011	4.010	4.000	4.000	3.996	4.000	4.000	4.000	4.000	4.000	4.000	4.000	4.000	4.000	4.001	4.000	4.000	4.000	4.000	4.009	4.007
		pair		vein	pair		pair		pair		pair		core	pair		pair		*	pair		pair *			pair *	
Jd (%)	99.6	89	57	25	96	48	50	94	99	50	96	51	98	89	36	97	48	41	94	57	76	37	11	95	50
Di	0.1	~4	28	44	1.4	38	41	4	0	38	1.5	31	0.6	4.2	14	1.5	41	42	3	37	9	33	70	0	46
Hd	<0.1	~2	>1	0	0	1	1.6	1	0	8	0.9	7	0	3.9	22	0.2	2.4	3	0.1	1.4	1.6	13	9	0	0
Ae	0	>1.4	10	25	2	11	7	1	0	3	1.1	9	0.1	0.5	28	1	6.7	3.7	2.2	38	10	46	5	0.2	1.6
Quad	0.2	8	34	46	1.4	40	43	4	1	46	2.9	38	1	9	36	2	44	46	3.1	3.4	12	15	81	1	46
MMF	0.6	0.64	0.81	0.98	0.98	0.98	0.99	1	0.28	0.83	0.45	0.8	0.57	0.42	0.4	0.6	0.93	0.85	0.99	0.96	0.68	0.75	0.84	0.99	1
MMF_T	0.6	0.56	0.63	0.63	0.77	0.41	0.73	0.89	0.28	0.78	0.33	0.65	0.55	0.4	0.23	0.43	0.81	0.79	0.58	0.88	0.39	0.55	0.79	0.91	0.98

MMF= $Mg/(Mg+Fe^{2+})$, $MMF_T = Mg/(Mg+Fe_{total})$; * $NaTi_{0.5}(Mg,Fe)_{0.5}Si_2O_6$ component = ~10% (KT02-3), 6.4% (Omp-MVE03-77-1), 5.6 & 3.4% (MVE04-20-1)

Ae: Aegirine, Aug: Augite, Omp: Omphacite, Di: Diopside, Hd: Hedenbergite, Jd: Jadeite, Omp: Omphacite, Quad: quadrangular components (diopside+hedenbergite+clinoenstatita+clinoferrosilite)

stringers of grossular are also associated with the late albite (Fig. 5C). This is the only recorded occurrence of pumpellyite north of the Motagua fault.

Mineral compositions

Pyroxene

Pyroxene compositions have been measured for a large number of rocks ranging from light-colored through variable green and even lavender jadeitites toward darker green mixed jadeite-omphacite jadeitites to omphacitites. Representative compositions for jadeite and omphacite (and coexisting pairs) from individual samples are presented in Table 1 (a growing database of compositions, images, and plots can be found at the senior author's research website). Figure 6A presents a sampling of compositions for clinopyroxenes in an individual jadeitite from north of the Motagua fault to demonstrate the range measured in a single sample, as well as portray the ranges among several rocks from the westernmost, central, and easternmost sources. The compositional variation is represented as broad lines where there is a continuous variation, both in jadeite and omphacite. This approach makes it easier to show the fundamental compositional variation among the four primary compositional components: jadeite - diopside – hedenbergite – aegirine. Adjacent jadeite-omphacite, either as omphacite inclusions in jadeite grains or immediate contact of omphacite overgrowths on jadeite, are shown with tie-lines. One important caveat in these data is that, although we have tried to take into account analyses that represent beam overlap between two pyroxenes which yield reasonable stoichiometry, some instances of reported compositions in plots that are actually mixtures, particularly for omphacite or diopside, cannot be ruled out without a much greater density of data than we have collected for all samples. A few characteristics of compositions and zoning are worth pointing out.

Jadeite compositions typically range from nearly pure jadeite to perhaps $Jd_{\sim 80\text{-}85}Di_{5\text{-}10}Ae_5Hd_2$, although some samples have a smaller range restricted toward pure jadeite and in others aegirine is the next most abundant component, rather than diopside. The Saltán lavender jadeite is distinctive for its very low iron content (<1wt%) consistent with enabling the Mn chromophore for the lavender color (*c.f.*, Ouyang, 2001; Nassau and Shigley, 1987), as well as minimal Ca content (diopside + hedenbergite ≤2mol%), and no coexisting omphacite.

Zoning patterns in jadeite grains vary considerably, particularly between different samples, but two general patterns are common. Most commonly grains contain relatively jadeite-rich crystal cores, with subtle cryptic

zoning and cluttered with inclusions as described above, surrounded by overgrowths richer in other components, particularly diopside. (Fig. 7A). Somewhat less common are cryptically zoned interiors of variable composition with or without an overgrowth of rhythmically zoned jadeite (Fig. 7B). Superimposed or overprinted on these patterns can be numerous "inclusions" of albite, analcime, paragonite, omphacite or some combinations of these, as described above. These observations are consistent with prior descriptions (Harlow, 1994; Sorensen et al., 2006) but different, in particular, from the recent description of jadeitite from the Sierra del Convento region, Cuba (García-Casco et al., 2009; see discussion).

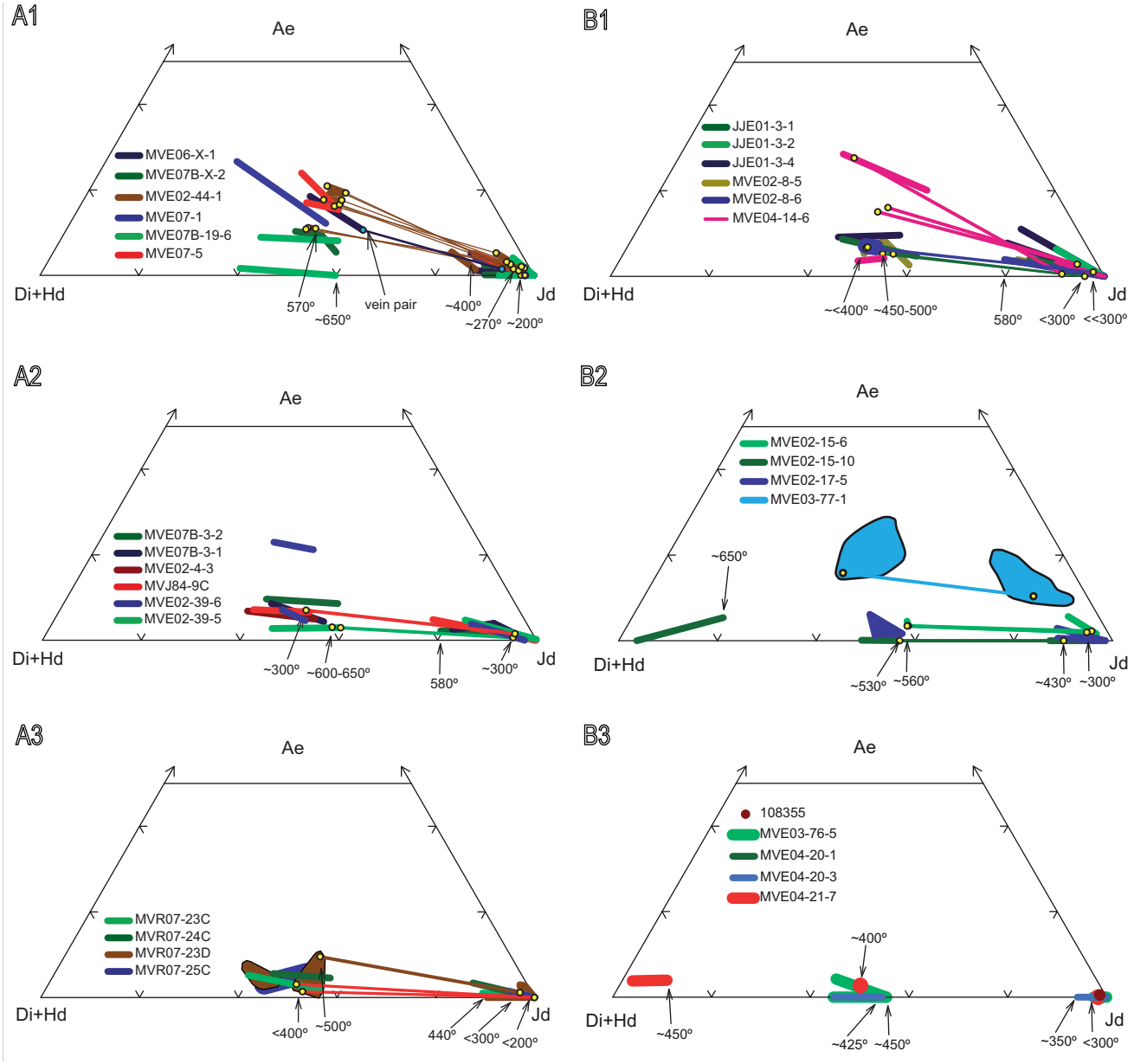

FIGURE 6 | **Plot of pyroxene compositions (molar components) in jadeitites. A) Samples north of the Motagua fault. A1: westernmost, A2: Central zone, A3: easternmost B) Samples south of the Motagua fault. B1: Carrizal Grande, B2: La Ceiba, B3: La Ensenada. Broad lines are representative of the zoning in jadeite and omphacite; individual compositions may scatter more broadly about the line but the width is indicative of the most prominent trend and the range of scatter. Samples with broader scatter (*e.g.*, MVE03-77-1 in B2) are shown with colored areas. However, where lines will obscure one another, lines have been made thinner for clarity. Fine lines and colored dots represent adjacent compositions of jadeite and omphacite. Temperature estimates are derived from pseudobinary section solvi calculations (García-Casco et al., 2009) for nearest Jd to Di_{100}, $Di_{90}Hd_5Ae_5$, $Di_{80}Hd_{10}Ae_{10}$, or $Di_{70}Hd_{15}Ae_{15}$ section. Ae: Aegirine, Di: Diopside, Hd: Hedenbergite, Jd: Jadeite.**

TABLE 2 | **Representative analyses of micas in jadeitite from north and south of the Motagua Fault**

	NORTH									SOUTH								
Wt%	MVE07-2	MVE02-39-6		MVE04	MVE07B-19-1		MVE06-X-1	MVR07-23D		MVE02-8-5			JJE01-X-3	JJE01-3-2	MVE03-77-5-1	MVE04-20-1	108355	
	Ph	Ms	Phl	Pg	Ms	Ms	Prs	Ph	Pg	Ph	Ph	Ba-Ph	Ba-Ph	Bio	Ph	Phl	Ph	Ba-Ph
SiO_2	51.79	43.79	39.26	48.55	48.38	44.67	30.91	51.06	48.30	54.25	57.24	54.71	47.31	39.09	54.77	41.07	50.34	46.27
TiO_2	0.09	0.01	0.27	0.07	0.03	0.04	0.04	0.07	0.04	0.28	0.26	0.23	0.25	0.14	0.14	0.02	0.00	0.03
Cr_2O_3	0.00	0.03	0.01	0.00	0.02	0.00	0.00	0.00	0.00	0.00	0.01	0.01	0.00	17.49	0.00	0.00	0.08	0.07
Al_2O_3	26.43	36.52	18.45	38.66	35.49	35.76	35.19	27.79	39.41	24.78	21.07	23.75	27.90	0.00	23.40	17.91	33.09	35.90
Fe_2O_3*	0.00	0.00	0.00	0.00	0.00	0.00	0.00	0.00	0.00	0.00	0.00	0.00	0.00	0.00	0.00	0.00	0.00	0.00
FeO	1.41	0.14	3.29	0.40	0.02	0.32	2.48	1.31	0.48	3.57	1.38	2.09	1.38	15.85	1.86	1.31	0.32	0.15
MnO	0.03	0.09	0.42	0.00	0.00	0.00	0.50	0.00	0.00	0.00	0.03	0.02	0.00	0.25	0.01	0.00	0.01	0.00
MgO	3.95	0.18	21.63	0.26	0.25	0.72	19.16	3.72	0.35	3.27	6.49	4.96	3.67	13.03	5.15	23.54	1.35	0.43
CaO	0.01	0.26	0.09	0.12	0.00	0.01	0.06	0.00	0.14	0.00	0.02	0.00	0.03	0.07	0.00	0.16	0.00	0.01
BaO	1.34	0.02	0.55	0.19	0.21	3.76	0.03	0.79	0.06	0.21	0.48	1.50	6.98	0.09	1.03	0.06	0.12	2.31
Na_2O	0.27	0.41	0.49	7.37	0.06	0.55	7.52	0.43	6.97	0.13	0.00	0.05	0.19	0.10	0.12	0.15	0.06	0.22
K_2O	10.13	10.36	9.67	0.50	11.43	9.50	0.09	10.73	0.86	10.16	9.72	9.15	8.66	9.36	9.64	9.97	10.27	9.97
H_2O*	4.49	4.36	4.19	4.74	4.56	4.42	4.43	4.51	4.76	4.56	4.62	4.56	4.35	4.04	4.55	4.27	4.59	4.48
Total	99.96	96.17	98.33	100.87	100.45	99.75	100.41	100.41	101.37	101.21	101.31	101.03	100.71	99.50	100.66	98.46	100.22	99.85
Cations per 20 Oxygen and 4 OH*																		
Si	6.914	6.023	5.614	6.140	6.359	6.065	4.183	6.785	6.081	7.135	7.435	7.191	6.529	5.796	7.214	5.765	6.583	6.192
$^{[4]}$Al	1.086	1.977	2.386	1.860	1.641	1.935	3.817	1.215	1.919	0.865	0.565	0.809	1.471	2.204	0.786	2.235	1.417	1.808
$^{[6]}$Al	3.072	3.943	0.723	3.903	3.856	3.787	1.795	3.137	3.929	2.976	2.659	2.869	3.066	0.852	2.846	0.729	3.684	3.854
Ti	0.010	0.001	0.029	0.007	0.003	0.004	0.004	0.007	0.004	0.027	0.025	0.022	0.026	0 .016	0.014	0.002	0.000	0.003
Cr	0.000	0.004	0.001	0.000	0.002	0.000	0.000	0.000	0.000	0.000	0.001	0.001	0.000	0.000	0.001	0.000	0.008	0.008
Fe^{3+}	0.000	0.000	0.000	0.000	0.000	0.000	0.000	0.000	0.000	0.000	0.000	0.000	0.000	0.000	0.000	0.000	0.000	0.000
Fe^{2+}	0.158	0.016	0.393	0.043	0.002	0.036	0.280	0.146	0.051	0.393	0.150	0.230	0.159	1.965	0.204	0.154	0.035	0.017
Mn	0.003	0.010	0.051	0.000	0.000	0.000	0.057	0.000	0.000	0.000	0.004	0.002	0.000	0.031	0.001	0.000	0.001	0.000
Mg	0.786	0.037	4.611	0.050	0.049	0.146	3.865	0.737	0.066	0.641	1.256	0.971	0.755	2.880	1.011	4.926	0.263	0.086
Ca	0.001	0.038	0.014	0.017	0.000	0.001	0.009	0.000	0.019	0.000	0.003	0.000	0.004	0.011	0.000	0.024	0.000	0.001
Ba	0.070	0.001	0.031	0.009	0.011	0.200	0.001	0.041	0.003	0.011	0.024	0.077	0.377	0.005	0.053	0.003	0.006	0.121
Na	0.071	0.108	0.137	1.807	0.015	0.145	1.972	0.111	1.701	0.033	0.000	0.012	0.052	0.028	0.030	0.040	0.016	0.057
K	1.725	1.819	1.765	0.081	1.916	1.645	0.016	1.819	0.138	1.705	1.610	1.535	1.524	1.770	1.619	1.785	1.714	1.702
Sum	13.896	13.977	15.753	13.916	13.855	13.965	16.001	13.997	13.911	13.786	13.733	13.721	13.965	15.559	13.780	15.663	13.727	13.850
OH *	4	4	4	4	4	4	4	4	4	4	4	4	4	4	4	4	4	4
MMF	0.83	0.7	0.92	0.54	0.96	0.8	0.93	0.83	0.56	0.62	0.89	0.81	0.83	0.59	0.83	0.97	0.88	0.84

MMF= $Mg/(Mg+Fe^{2+})$

* OH is calculated to fill univalent anion site and H_2O is back calculated from the conversion of ions to wt%

Bio: Biotite, Ba-Ph: Ba-Phengite, Ms: Muscovite, Pg: Paragonite, Ph: Phengite, Phl: Phlogopite, Prs: Preiswerkite

Omphacite is most common as overgrowths on and veins cutting through jadeite. In the former case, compositions of contacting jadeite and omphacite usually approach that of equilibrium pairs (more discussion below), but in the latter case, there is zoning across the omphacite vein (Fig. 7C) in which a portion or even all of the vein omphacite does not appear to be in equilibrium with adjacent jadeite (also discussed below). Omphacite compositions trend away from that potentially in equilibrium with jadeite toward more diopside + hedenbergite + aegirine-rich compositions. The compositions of omphacite inclusions and overgrowths generally overlap in each thin section, although some omphacite inclusion compositions are much higher in aegirine content (Fig. 6A) than is consistent with interpretations of coexisting sodic pyroxenes (Green et al., 2007). In addition, most coexisting jadeite-omphacite compositions do not follow the Green et al. (2007) solvus (see discussion below).

There is a trend displayed among the three different regional clusters of jadeitite indicating higher aegirine component in the compositions of omphacite and jadeite (trending away from the cores of jadeite grains) for the westernmost samples that decreases further eastward. In addition, there is a trend toward a smaller jadeite - omphacite compositional gap in jadeitite from the west as compared to those from further east (Fig. 6A; Table 1).

The green color of jadeite and omphacite is mostly related to iron content, although no study has been carried out to accurately evaluate the ferrous-ferric variation or its impact on color. Chromium has been shown clearly to yield the color in so-called imperial jade (see Harlow et al., 2007), and likely contributes to color in impure jadeite and omphacite (Table 1, Sorensen et al., 2006; Harlow and Olds, 1987).

Mica

Representative mica compositions are presented for only the new localities from north of the Motagua fault in Table 2, as details of mica composition were presented in Harlow (1995). Paragonite has a nearly ideal end-member composition. Phengitic muscovite is less common than paragonite in jadeitite north of the Motagua fault, with maximum Si atoms per formula

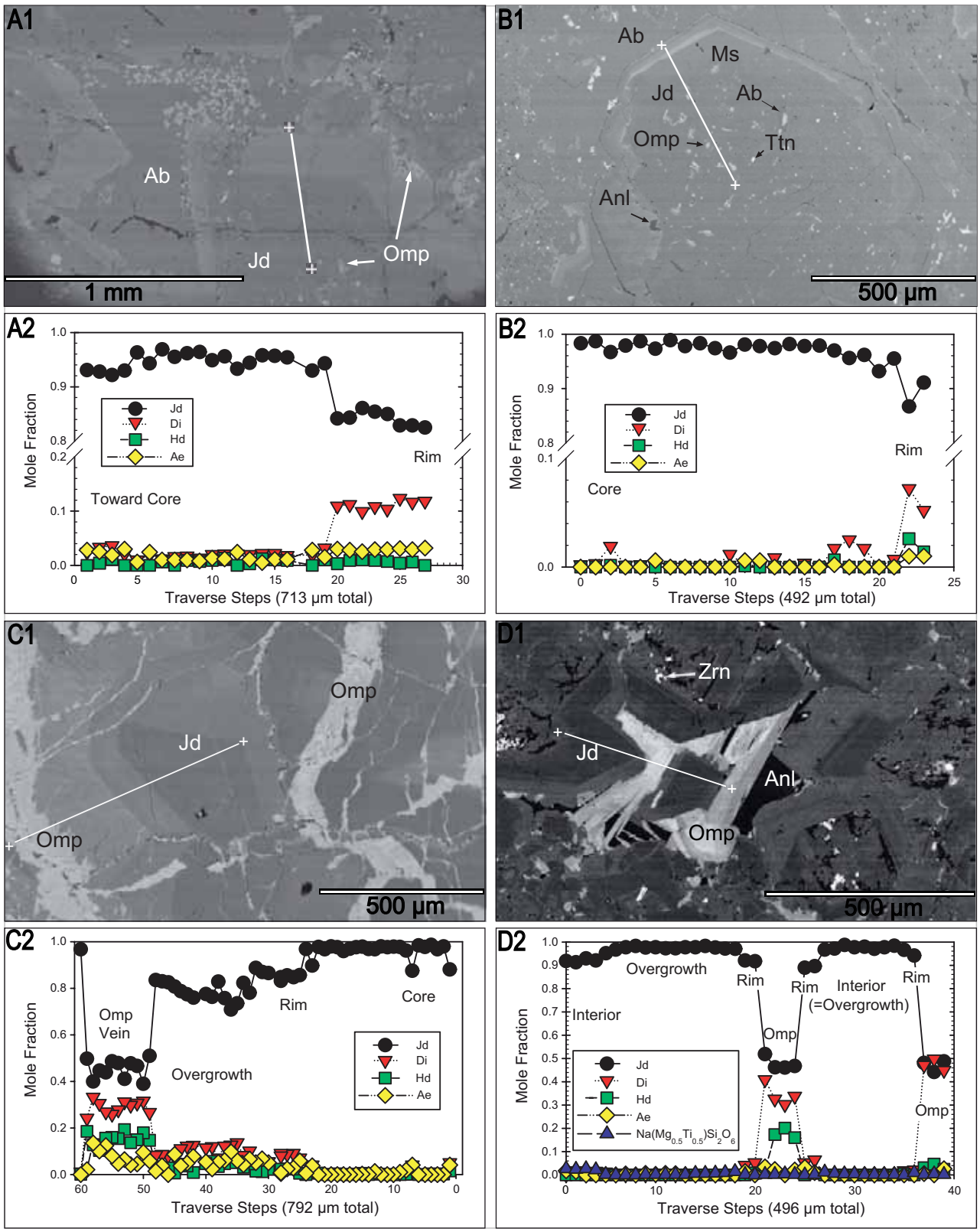

FIGURE 7 | **Plot of pyroxene components from microprobe traverses of grains, overgrowths and veins in jadeitite. BSE images show traverse (+ sign at ends) and phase labels. A) Traverse across jadeite grain with cryptically zoned interior and a more diopside-rich overgrowth: MVE04-44-1, Quebrada de los Pescaditos; B) Traverse across jadeite grain with relatively uniform interior containing inclusions toward diopsidic rim: MVR07-23C, Aldea Las Cruces; C) Traverse of a omphacite vein in a jadeitite: MVJ84-12-2, Río La Palmilla; D) Traverse of rhythmic overgrowths of jadeite-rich and jadeite-poorer compositions in MVE04-15-3, La Ceiba. Ab: Albite, Ae: Aegirine, Anl: Analcime, Di: Diopside, Hd: Hedenbergite, Jd: Jadeite, Ms: Muscovite, Omp: Omphacite, Ttn: Titanite, Zrn: Zircon.**

unit (apfu)<7 and Mg/(Mg+Fe^{2+})>0.7 (Fe^{2+} as determined by stoichiometry and charge balance). Muscovite (low Mg+Fe^{2+}) is comparatively rare as inclusions, but is most common in the latest stage of crystallization of lavender jadeitite from near Saltán; phengite occurs with jadeite in less altered areas. Phlogopite is less common than either paragonite or phengite in jadeitite but increases in abundance with that of omphacite in the jadeitite-omphacitite rocks; Mg/(Mg+Fe^{2+}) values range between 0.69 and 0.93 with variation typically limited to <0.04 in single samples. Assemblages and even interlayering of the three micas has been found in several samples (see Table I, Electronic Appendix). As described by Harlow (1994) preiswerkite occurs as a late-stage alteration of paragonite with Mg/(Mg+Fe^{2+}) varying distinctly between different rocks and even different localities, from a rare low of 0.75 to a more common 0.93-0.95.

Amphibole

Representative amphibole compositions are presented in Table 3. As also reported by Harlow (1994), all amphibole in jadeitite is late-stage taramitic amphibole, both magnesian and ferroan, which appears to reflect the composition of the late omphacite (late fluid), at least in terms of MgO/(MgO+FeO_{Total}), (Mg/(Mg+Fe_T)) as ferrous-ferric evaluation is only assessed here by stoichiometry.

Other Calcic Minerals

Grossular garnet was described in some of the taramite - omphacite rocks associated with jadeitite north of the Motagua fault (Harlow, 1994). Grossular (see above) is otherwise only found as a late phase in the lavender jadeitite from near Saltán. A single specimen of jadeitite/omphacitite near Manzanal originally collected by Zenaide Carvalho da Silva (ZC-20, see Silva, 1967, 1970) contains garnet somewhat like that of garnet amphibolites in the area but with spessartine-rich rims (Table 4). This sample is the best (and a rare) argument for metasomatic replacement of a metamorphic rock (e.g., pelitic or mafic) by jadeitite, although there is only this relict phase rather than a textural indication. Pumpellyite-Mg and vesuvianite are newly described north of the Motagua fault from Saltán jadeitite coexisting with albite, grossular, Sr-rich zoisite, allanite, K-feldspar, and phengite. Vesuvianite has recently been described by Nyunt et al. (2009) in jadeitite from the Jade Tract in Myanmar, and the compositional characteristics are very similar to that in Guatemalan jadeitite, that is, high in Ti (up to ~5wt% TiO_2) and Na (up to ~2.5wt% Na_2O; Table 4). We concur with their conclusions of composition influenced by sodic-metasomatic-HP/LT formation, however, whereas Nyunt et al. (2009) argue that vesuvianite grew in equilibrium with jadeite, textures for Guatemalan jadeitite clearly show vesuvianite to be secondary, in later veins and overgrowth selvages with the phases noted above. Pumpellyite is aluminous but still should be classified as pumpellyite-Mg. For this reason the analyses in Table 4 are normalized to 3 Si cations, which results in a ~45-50% pumpellyite-Al component, and a large cation site (Ca+Na) that contains a small proportion of vacancies (~<0.05 atoms per formula unit). Both zoisite and clinozoisite are found, generally as late stage phases as described by Harlow (1994), with Al/(Al+Fe+Mn+Cr) ranging from 0.80 to 0.99. As described in Harlow (1994) Sr can reach significant concentrations in zoisite (see Table 4), particularly in the alteration of lavender jadeitite from Saltán, and appears to be concentrated in this calcic phase among those listed above, whether by crystal-chemistry or growth stage in jadeitite evolution/alteration. Allanite–REE-rich clinozoisite/zoisite compositions require further study, but appear to be Ce-rich with ~≥20wt% total REE-oxide (0.13 apfu).

Jadeitite texture and mineralogy South of the Motagua fault

Jadeitites from this area are distinct for the three zones recognized at this time. Consequently, we describe them separately.

Carrizal Grande

This jadeitite is generally not so granoblastic, with more columnar or interfingered jadeite quasi-prisms, and massive in appearance, with smaller grain size, on average, than the jadeitite found north of the Motagua fault. Maximum grain size for jadeite is generally <2mm whereas tabular phengite grains can exceed 5mm across. Interiors of jadeite grains can contain dense clusters of small inclusions (<10μm), typically omphacite, phengite, quartz, lawsonite, 1 or 2-phase fluids as well as titanite, zircon, and apatite as crystals, clusters, or blebs. Outside of the cores jadeite grains tend to be free of inclusions (Fig. 5D-F), except near the grain boundaries. As observed in BSE images, the interiors of grains typically exhibit subtle, patchy compositional zoning, while rims are rhythmically zoned or nearly unzoned. Most grain boundaries between jadeite and other primary minerals do not show interstitial coatings or abundant veining. When jadeite rims have inclusions, they typically are enveloped as individual phengite, titanite, rutile, and/or zircon grains. Veins, when present, tend to be sharp and cross-cutting and can consist of omphacite, albite, quartz, and cymrite; quartz veins can be in direct contact with jadeite. In jadeitite from Quebrada Seca, omphacite veins are common and demonstrate several generations based on zonation across the vein (Fig. 5G) and envelopment of earlier omphacite vein

TABLE 3 | **Representative amphibole compositions in jadeitite from Guatemala**

	Tar	Tar	Ftar	Ftar	Gln	Gln	Act	Act	Act
	MVE03	MVE07	ZC-20	MVJ84	JJE01	MVE02	MVE02	MVE02	MVE03
	81-3	7	39-6	44-2	3-4	14-5	14-5	15-10	77-5-1
SiO_2	42.57	43.00	43.12	41.07	59.24	59.96	57.08	57.44	58.66
TiO_2	0.26	0.67	0.47	0.51	0.03	0.00	0.01	0.01	0.09
Cr_2O_3	0.00	0.00	–	0.00	0.00	0.03	0.00	0.02	0.08
Al_2O_3	20.17	19.34	15.28	16.34	11.61	11.88	0.31	0.26	3.37
Fe_2O_3	3.62	0.00	2.64	4.04	1.20	0.02	0.03	0.00	0.00
FeO	5.25	10.91	15.01	16.71	3.68	3.98	5.16	5.78	7.03
MnO	0.37	0.16	0.59	0.28	0.08	0.07	0.34	0.06	0.10
MgO	11.35	9.24	7.22	5.29	13.01	13.41	20.61	20.39	16.48
CaO	7.33	6.70	6.50	7.03	0.30	0.17	12.98	12.81	10.20
BaO	0.00	0.00	–	0.02	0.02	0.02	0.03	0.00	0.00
Na_2O	6.44	6.72	5.98	5.49	7.47	7.26	0.35	0.13	2.07
K_2O	0.36	0.40	0.74	0.84	0.05	0.03	0.04	0.14	0.11
H_2O*	2.10	2.06	2.01	1.98	2.22	2.24	2.14	2.15	2.18
TOTAL	99.82	99.20	99.54	99.60	98.92	99.06	99.09	99.18	100.37
Cations per 22 O + 2(OH)*									
Si	6.073	6.253	6.442	6.221	7.989	8.036	7.987	8.027	8.077
$^{[4]}Al$	1.927	1.747	1.558	1.779	0.011	0.000	0.013	0.000	0.000
$^{[6]}Al$	1.464	1.567	1.132	1.138	1.835	1.876	0.039	0.042	0.547
Ti	0.028	0.073	0.052	0.058	0.003	0.000	0.001	0.001	0.009
Cr	0.000	0.000	0.000	0.000	0.000	0.003	0.000	0.002	0.008
Fe^{3+}	0.389	0.000	0.297	0.461	0.122	0.002	0.004	0.000	0.000
Fe^{2+}	0.626	1.327	1.875	2.117	0.415	0.446	0.604	0.675	0.810
Mn	0.045	0.020	0.074	0.035	0.009	0.008	0.040	0.007	0.012
Mg	2.415	2.003	1.607	1.195	2.616	2.680	4.299	4.248	3.382
Sum C	4.966	4.990	5.037	5.004	4.999	5.015	4.986	4.975	4.769
Sum C-	0.000	0.000	0.037	0.004	0.000	0.000	0.015	0.000	0.000
Ca	1.121	1.044	1.040	1.141	0.043	1.946	0.025	1.918	1.505
Na	0.913	0.967	0.923	0.855	1.953	0.068	1.888	0.035	0.553
Sum B	2.034	2.010	2.000	2.000	1.996	2.014	1.928	1.954	2.058
Na	0.867	0.926	0.808	0.757	0.000	0.028	0.000	0.000	0.000
K	0.065	0.074	0.140	0.163	0.009	0.008	0.004	0.025	0.019
Sum A	0.932	1.001	0.948	0.920	0.009	0.036	0.004	0.025	0.019
TOTAL	15.932	16.001	15.948	15.920	15.005	15.036	14.968	14.981	14.923
OH *	2.000	2.000	2.000	2.000	2.000	2.000	2.000	2.000	2.000
MMF	0.79	0.60	0.46	0.36	0.86	0.86	0.88	0.86	0.81
MMF_T	0.70	0.60	0.43	0.32	0.83	0.86	0.88	0.86	0.81

$MMF=Mg/(Mg+Fe^{2+})$, $MMF_T=Mg/(Mg+Fe_{total})$

Act: Actinolite, Ftar: Ferrotaramite, Gln: Glaucophane, Tar: Taramite

* OH is calculated to fill the univalent anion site, and H_2O is back calculated from the conversion of ions to wt%.

fragments by later growths. These omphacite veins can color the rock an intense blue-green (desirable as "blue jade") that is correlated with relatively high TiO_2 content in the omphacite (≤2.0wt% see Table 1 and Harlow et al., 2004b). Phengite grains are typically zoned by an overgrowth of barian rims (Fig. 5G), but occasionally have a more complex pattern or cryptic internal zoning. These grains are generally free of inclusions, although titanite and zircon are most common if encountered, and phengite grain clusters can envelope jadeite and other mineral grains. Titanite grains can vary from a few microns to over 1mm across, and larger ones commonly have a small nucleus of rutile or zircon (MVE02-8-5) and can include jadeite or phengite (MVE07-9). Titanite abundance appears to be correlated with the abundance of omphacite as well as the saturation of green color of the rock. Textures of titanite vary considerably, from larger nematoblasts (to 1mm), smaller quasi-euhedral crystals, and lacework growths around other phases, such as jadeite, omphacite, phengite, etc (Fig. 5H). Zircons are generally small (<150μm long) and vary from well-defined crystals, sometimes in delicate clusters, to rounded blebs; inclusions observed to date are only cavities, presumably fluid inclusions. Zircon abundance and crystal size appears to be correlated with the abundance of phengite. Allanite has been found in several jadeitites as discrete crystals along jadeite-phengite grain boundaries to a ~75μm maximum

TABLE 4 | **Representative analyses of other calcic minerals in jadeitite north and south of the Motagua Fault**

	NORTH									SOUTH									
	MVE07B-19-1	ZC-20		MVE07B-19-4	MVE07B-19-1	MVE07B-19-4		MVE07B-19-1		MVE06-17-2		MVE04-20-1	MVE03-77-4	MVE02-17-5		MVE03-76-5	MVE04-30-1	JJE01-X-3	JJE01-6-1
Wt%		Garnet		Vesuvianite	Pumpellyite	Zoisite		Clinozoisite	Allanite	Garnet			Vesuvianite			Pumpellyite		Lawsonite	
SiO_2	39.42	36.22	36.40	34.43	37.48	38.78	38.01	34.79	30.94	37.07	37.06	39.57	36.49	37.73	37.86	38.26	37.90	38.07	37.39
TiO_2	0.30	0.07	0.15	1.55	0.22	0.28	0.27	0.09	0.27	0.37	0.09	0.17	4.51	3.92	5.89	0.03	0.01	0.05	0.89
Al_2O_3	21.84	21.13	20.27	17.95	26.44	32.43	31.22	25.96	18.29	0.03	0.00	22.32	17.86	18.61	17.62	26.36	25.95	31.50	30.67
Cr_2O_3	0.00	–	–	0.00	0.03	0.00	0.01	0.08	0.20=Y_2O_3	20.56	20.98	0.00	0.00	0.04	0.01	0.01	0.00	0.00	0.03
Fe_2O_3	0.74	1.36	1.13	–	–	0.23	0.75	5.41	26.62=LREE‡	0.58	0.49	0.03	–	1.63	1.60	–	–	0.10	0.42
FeO	0.17	17.42	22.39	1.50	2.34	–	–	–	9.55	26.84	30.39	0.00	1.87	0.00	0.00	0.52	0.13	–	–
MnO	0.48	12.55	2.98	0.00	0.08	0.00	0.00	0.10†	0.00	7.79	1.29	0.02	0.09	0.06†	0.08†	0.02	0.00	0.00	0.00
MgO	0.03	1.23	0.56	0.27	2.50	0.00	0.02	0.03	0.30	0.62	1.04	0.07	0.36	0.58	0.35	3.93	4.50	0.00	0.01
CaO	36.32	9.30	13.61	29.34	22.76	23.42	20.30	12.57	11.58	6.41	8.56	37.61	31.94	31.42	30.56	22.96	23.77	17.30	17.03
SrO	0.02	–	–	–	0.05	2.53	7.18	17.63	0.02	–	–	0.00	–	0.26	0.30	–	0.00	0.32	0.66
BaO	0.00	–	–	0.03	0.00	0.00	0.05	0.16	–	0.03	0.05	0.00	0.00	0.00	0.00	0.00	0.00	0.02	0.00
K_2O	0.01	0.01	0.01	0.00	0.50	0.02	0.02	0.00	–	0.19	0.04	0.02	2.01	2.71	3.08	0.47	0.09	0.01	0.00
Na_2O	0.00	0.06	0.01	1.05	0.04	0.00	0.00	0.03	–	0.00	0.00	0.00	0.00	0.01	0.03	0.00	0.00	0.00	0.00
H_2O*	–	–	–	3.64	6.65	1.94	1.90	1.75	1.56	–	–	–	2.53	3.18	3.18	7.19	6.84	11.41	11.21
TOTAL	99.33	99.34	97.53	89.76	99.09	99.64	99.73	98.62	99.84	100.49	99.98	99.83	97.67	100.00	100.39	99.75	99.18	98.78	98.31
Cations pe	24 O	24 O	24 O	18 Si	3 Si	25 O	25 O	25 O	25 O	24 O	24 O	24 O	18 Si	18 Si	18 Si	3 Si	3 Si	4 Si	4 Si
[4]Si	5.977	5.855	5.950	18.000	3.000	5.979	5.997	5.967	5.935	5.981	5.961	5.960	18	18	18	3	3	4	4
[4]Al	0.023	0.145	0.050	0.000	0.000	0.021	0.003	0.033	0.065	0.019	0.039	0.040	0	0	0	0	0	0	0
SumTet	6.000	6.000	6.000	18.000	3.000	6.000	6.000	6.000		6.000	6.000	6.000	18	18	18	3	3	4	4
[6]Al	3.880	3.879	3.855	11.060	2.494	5.872	5.803	5.215	4.069	3.890	3.940	3.922	10.382	10.465	9.874	2.436	2.421	3.901	3.867
Ti	0.034	0.009	0.018	0.609	0.013	0.032	0.031	0.012	0.039	0.045	0.011	0.019	1.672	1.406	2.105	0.002	0.001	0.004	0.072
Cr	0.000	–	–	0.000	0.002	0.000	0.001	0.011	0.071=Y_2O_3	0.004	0.000	0.000	0.000	0.017	0.005	0.001	0.000	0.000	0.003
Fe3+	0.085	0.165	0.140	–	–	0.027	0.089	0.698	1.829=LREE‡	0.071	0.059	0.003	–	0.587	0.574	–	–	0.008	0.034
Fe2+	0.022	2.355	3.061	0.657	0.157	–	–	–	1.532	3.620	4.089	0.000	0.769	0.000	0.000	0.034	0.008	–	–
Mn	0.061	1.718	0.413	0.000	0.005	0.000	0.000	0.014†	0.000	1.064	0.175	0.003	0.039	0.023†	0.029†	0.002	0.000	0.000	0.000
Mg	0.006	0.295	0.136	0.211	0.298	0.000	0.006	0.007	0.086	0.148	0.249	0.017	0.267	0.414	0.247	0.459	0.530	0.000	0.002
Ca	5.900	1.610	2.384	16.436	1.952	3.869	3.432	2.311	2.380	1.108	1.475	6.070	16.882	16.059	15.568	1.929	2.016	1.947	1.952
SrO	0.001	–	–	–	0.002	0.226	0.657	1.753	0.002	–	–	0.000	–	0.071	0.083	–	0.000	0.020	0.041
Ba	0.000	–	–	0.000	0.000	0.000	0.003	0.011	–	0.002	0.003	0.000	0.000	0.000	0.000	0.000	0.000	0.001	0.000
Na	0.003	0.019	0.004	1.065	0.076	0.007	0.005	0.000	–	0.060	0.011	0.007	1.924	2.509	2.837	0.073	0.013	0.003	0.000
K	0.000	0.002	0.002	0.000	0.004	0.000	0.001	0.007	–	0.000	0.000	0.000	0.000	0.007	0.017	0.000	0.000	0.000	0.000
Total	15.991	16.053	16.013	48.043	8.004	16.032	16.027	16.039	16.008	16.011	16.014	16.042	49.935	49.340	49.340	7.936	7.990	9.884	9.972
OH*	–	–	–	12.701	1.551	2	2	2	2	–	–	–	8.329	9.494	9.483	1.76	1.61	4	4
H_2O*	–	–	–	–	–	0	0	0	0	–	–	–	–	–	–	–	–	2	2
										core	rim								

* OH and H_2O calculated from stoichiometry or charge balance; H_2O wt% back calculated from stoichiometry; † Fe or Mn is recalculated as trivalent. ‡ LREE = La_2O_3 (3.33 wt%, 0.236 apfu) + Ce_2O_3 (10.47, Czo: Clinozoisite, Zo: Zoisite

dimension and surrounding/invading monazite grains of similar dimension in two samples.

Late-stage alteration is not as common as observed in jadeitites north of the Motagua fault. This is obvious from the generally greater translucency of the jadeitite due to tight grain boundaries lacking refractive-index contrast gaps or coatings. The most common grain-boundary infiltration phases, when observed, are quartz and albite, which can be accompanied by omphacite or cymrite. Quartz infiltrations have been observed in which jadeite grains, with somewhat "chewed up" rims, are separated by a quartz matrix and surrounded by blebs of omphacite and diopside (Fig. 5I).

La Ceiba

The jadeitite varies from a medium- to fine-grained, opaque, granoblastic texture to a darker translucent microcrystalline mesh texture omphacitite. However, the latter variety is cut by dense networks of fractures that render the material fragmental (and not suitable for use as gem jade). Jadeite grains have a similar texture as those in jadeitite from the Carrizal Grande area; grain interiors are decorated with blebs of omphacite, quartz and fluid inclusions. Small rounded zircon inclusions are also common in jadeite, but not generally in the areas of the previously mentioned inclusions (Fig. 5J). Zoning in jadeite grain interiors is subtle and generally patchy and cryptic, and rims are typically narrow, relatively unzoned with slightly lower jadeite content (brighter in BSE). Overgrowth of cryptically zoned core jadeite by clean rhythmic purer jadeite followed by less jadeite-rich, possibly multiple times, is observed in MVE04-15-3 (Fig. 7D). Coarser-grained omphacite, phengite, and titanite fill in around grains of jadeite in discontinuous, broken-up veins. Zoning in omphacite cores is cryptic but rims or outer regions can be rhythmically zoned. Large titanite grains (up to several mm) have an irregular shape and appear to have numerous quartz and fluid inclusions (voids in polished section). Late, light-colored veins transect the rock and typically consist of quartz, diopside, cymrite, vesuvianite (Fig. 4D; Fig. 5K) and, on occasion, pectolite. Albite appears between grain boundaries of jadeite.

La Ensenada

The jadeitite here is noted for its generally pale tan-to-grayish body color decorated by stringers of lavender, blue, emerald-green, and pink, earning it the name "rainbow jade". It consists of dense intergrowths of jadeite crystals cut by narrow pumpellyite-dominant veins, in turn cut by veins of grossular and albite. Jadeite crystals vary from lathy, generally <300μm long, to irregular to radial clusters forming a dense mat of jadeite. Veins crosscut the jadeite and mantle or infill the jadeite with blocky pumpellyite of similar but more equant grain size. The centers of the veins are occupied with grossular ± albite (Fig. 5L); however, pumpellyite + grossular ± albite is also found dispersed as small regions in the jadeitite in what appear to be late-stage veins. Pinkish grossular crystals are commonly intergrown, with individuals ranging from ~100μm to 1mm across, and cathodoluminescence reveals oscillatory zoning patterns (Fig. 5M – MVE04-20-1) not evident in BSE or in major elements. Omphacite is minor both as inclusions and overgrowths on jadeite grains. Phengite, titanite, apatite, chlorite, zircon, and celsian are other minor constituents of this rock type. Light brown chloritite veins cut through some samples and consist of Fe-poor (<1wt% FeO_T) clinochlore plus omphacite and titanite in decreasing abundance with distance from the jadeitite boundary.

Mineral compositions

Pyroxene

As with the samples from north of the Motagua fault, representative compositions are presented in Table 1, and summary plots are provided in Figure 6B, with plots for each of the three distinct source areas south of the Motagua fault. The following characteristics are noted:

1) As in the case of northern jadeitite, jadeite compositions typically range from pure jadeite to perhaps $Jd_{\sim 80\text{-}85}Di_{5\text{-}10}Ae_5Hd_2$, with some dispersion in diopside versus aegirine content. The La Ensenada jadeite, like the lavender jadeite from Saltán, is distinctive for its very low iron content (<1wt%), but does have minor coexisting omphacite and even diopside.

2) Zoning patterns in jadeite grains among individual jadeitites vary considerably, but the most common is a jadeite-rich core, either relatively homogeneous or with cryptic, patchy zoning, particularly when there are abundant inclusions, and a less jadeite-rich (more diopside + aegirine + hedenbergite) rim. In some samples, e.g., JJE01-3-1, well-formed crystals manifest coarse oscillatory zoning (from high-to-low-to-high jadeite content) usually terminated by a less jadeite-rich rim or an omphacite overgrowth (Fig. 5N).

3) The compositions of omphacite inclusions and overgrowths generally overlap in each thin section, however, the jadeite – omphacite gap tends to be larger for coexisting jadeite and omphacite at the cores of jadeite grains than at rims of those grains. And, as with samples from the North, some omphacite inclusion compositions are much higher in aegirine content (Fig. 6B; Table 1) than is consistent with the Green et al. (2007) solvus. Likewise, as with northern jadeitite, coexisting jadeite-omphacite compositions do not follow their solvus. Finally, there is the unusual Ti-rich compositions (*e.g.*, Table 1) of certain blue vein omphacite in samples from the Carrizal Grande area and even in jadeite from La Ensenada, which is best characterized by a $NaTi_{0.5}Mg_{0.5}Si_2O_6$ (rather than alumino-buffonite – $CaTi_{0.5}Mg_{0.5}AlSiO_6$) component (Table 1; Harlow et al., 2003, 2004b).

4) There are distinct differences in the pyroxene compositional arrays between the three different source areas south of the Motagua fault (Fig. 6B). In general, the range of compositions of both jadeite and omphacite are greatest for Carrizal Grande, intermediate for La Ceiba, and the smallest for La Ensenada. The most straightforward interpretation is a decrease in the maximum temperature of growth (equilibration) of jadeite and omphacite, in the order listed. Likewise, except for a single sample from La Ceiba (MVE03-77-1), the maximum aegirine content for both jadeite and omphacite varies in the same order, greatest at Carrizal Grande and least at La Ensenada. Finally, at La Ceiba and La Ensenada we found individual jadeitite samples (MVE02-15-10, MVE04-21-7) with late stage veining containing a diopside composition separated by a gap from omphacite compositions.

Mica

Representative mica compositions are presented for localities from south of the Motagua fault in Table 2. Muscovite grains analyzed are usually phengitic, with variable enrichments in Ba similar to values in muscovite north of the Motagua fault. However, Si apfu is significantly higher than in samples north of the Motagua fault, from the highest values at Carrizal Grande (≤7.5), lower at La Ceiba (≤7.2), and lowest at La Ensenada (<6.7) where mica is rare. At La Ensenada, mica is more likely to be phlogopite, but, if muscovite, it is not generally phengitic. Ba substitution for K follows the same mechanisms described by Harlow (1995) in mica north of the Motagua fault by which the predominant one ($BaAlK_{-1}Si_{-1}$) lowers Si content of the mica. Mg/(Mg+Fe) of phengite varies within and between jadeitite samples from 0.57-0.90 (MVE02-8-5) to a narrower 0.80-0.92 (JJE01-3-4), both samples from Carrizal Grande, with a similarity to those values (but perhaps slightly lower) in coexisting omphacite (jadeite cannot be well assessed for $Mg/(Mg+Fe^{2+})$ versus

$Mg/(Mg+Fe_T)$. This variability is not clear for jadeitite from La Ensenada, for lack of analyses, although $Mg/(Mg+Fe^{2+})$ of phlogopite is high 0.96-0.97 from a single sample (MVE04-20-1).

Amphibole

Representative amphibole compositions are presented in Table 3. Glaucophane is a rare late phase in jadeitite and more commonly associated with a rock composed principally of omphacite + glaucophane from the Carrizal Grande area, with composition essentially on the glaucophane – ferro - glaucophane join ($Mg/(Mg+Fe^{2+})$ 0.8-0.9 – see Table 3). Actinolite is found in veins, typically with quartz or albite and is near the tremolite-actinolite join in composition.

Other calcic minerals

Grossular garnet is common but only in the pumpellyite - jadeitite from around La Ensenada and is nearly pure end-member grossular. The zoning evident by cathodoluminescence does not manifest itself in microprobe analyses. Otherwise, a single specimen of garnet jadeitite infiltrated with quartz and lawsonite from Carrizal Grande (MVE06-17-2) contains garnet somewhat like that in eclogite in the area but with much greater spessartine content (to ~8wt% MnO, ~1.2Mn apfu: Table 4). This sample is the best (and a rare) argument for metasomatic replacement of an eclogite by jadeitite, without textural indication. If so, the high Mn content of garnet and high aegirine content (to 43mol%) and low jadeite content (4-10mol%) of minor omphacite (if relict) are not typical for local eclogite. Vesuvianite is found in late stage veins with cymrite and quartz at La Ceiba. As with compositional characteristics from the sample north of the Motagua fault, Ti is high (to >5wt% TiO_2) and Na (to ~2.5wt% Na_2O; Table 4). It also contains a small amount of SrO (0.25-0.5wt%, 0.07–0.14 Sr apfu). Pumpellyite-Mg is common in pumpellyite-jadeitite from near La Ensenada. Pumpellyite straddles the boundary between –Al and –Mg types with ~30-50% pumpellyite-Al and 40-50% pumpellyite-Mg components. Lawsonite is common in some jadeitites and omphacitites from the Carrizal Grande area, occurring in the mélange with lawsonite - eclogite. Lawsonite compositions are calculated with all iron and manganese, although minor, as trivalent cations, which still leaves the six-fold site slightly deficient when cations are normalized to 4 silicon atoms, as well as the oxide (plus calculated H_2O) and cation totals are somewhat low, even while including Sr content (typically 0.03–0.35 apfu; Table 4).

DISCUSSION

Estimates of crystallization P-T

As nearly monomineralic rocks are affected by episodes of growth and some alteration, assessing conditions of crystallization, particularly peak P-T, can be difficult. We have separated the interpretation into sections on phase assemblage and then jadeite-omphacite relationships as well as the distinctions between the tectonically distinct environments: north versus south of the Motagua fault in Guatemala.

PT conditions North of the Motagua fault

None of the jadeitites in this region contain quartz, either as inclusions in jadeite or in veins, but all contain albite, mica and usually analcime, which indicates they all formed at P lower than that of the jadeite + quartz stability field unless the phase assemblage represents a fully retrograded one, consistent with the earlier observations by Harlow (1994). The presence of zoisite/clinozoisite rather than lawsonite in the presence of paragonite suggests formation at T above the reaction lawsonite + jadeite = zoisite/clinizoisite + paragonite + albite + H_2O (Fig. 8). These constraints yield P=6-12kbar and T=300-450°C; higher temperatures are permissible if the activity of SiO_2 is much below unity (see Fig. 8 Harlow, 1994). The modest jadeite–omphacite gap (Green et al., 2007) yields temperatures from 200 to >500°C for pyroxene pairs, with indications of higher temperatures for samples from the more western localities and lower for ones from the east (see Fig. 6), except for those from Saltán. More discussion of these data are presented below.

Carpenter (1979, 1981) described antiphase domain structures <20nm in size in omphacite from a jadeitite that undoubtedly came from the central area North of the Motagua fault (presumably Manzanal). These omphacite antiphase domain textures indicate that the omphacite went through the order-disorder transformation soon after the omphacite crystallization in *C*2/*c* space group (presumably metastably). But more significantly, the very small antiphase domain size is consistent with the low-T formation of the jadeitite and a simple cooling history.

Alteration of jadeitite to the albitite assemblage, as described in Harlow (1994), involves both additional SiO_2 (as well as large ion lithophile elements (LILE)) via a fluid (see Sorensen et al., 2010), as well as a down P trajectory below the jadeite stability field, usually, into the zoisite stability field (T>350-400, see Fig. 8) and into the greenschist facies (350-450ºC at <7kbar). Moreover, the symplectitic textures of albite + analcime and albite + nepheline (also described by Tsujimori et al., 2004b) are further evidence of fluid involvement in these retrograde reactions:

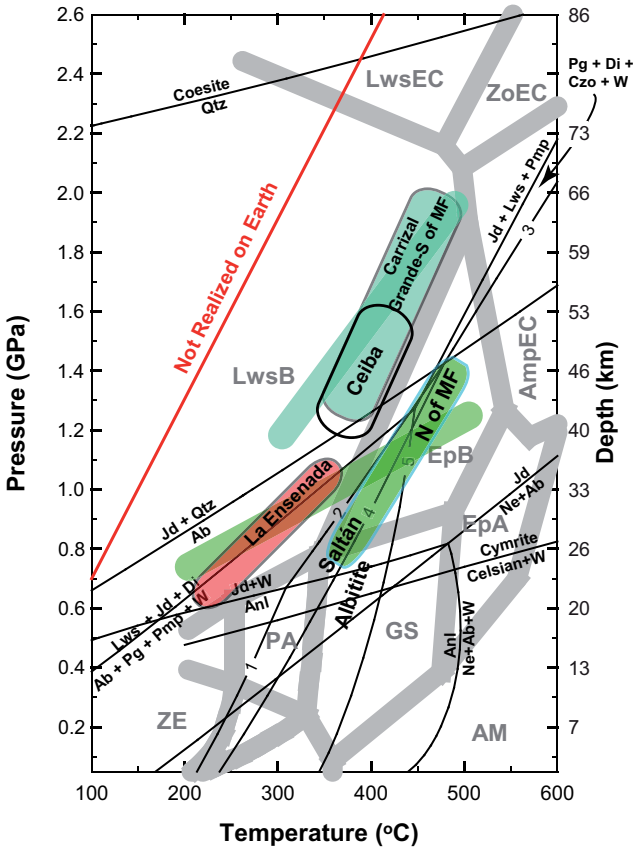

FIGURE 8 | **Plot of P-T grid with estimates for jadeitite formation. Conditions north of the fault (N of MF) are shown in green with the singular conditions at Saltán shown at the lower-left end of the distribution. Conditions south of the fault are shown in blue-green for Carrizal Grande, an outlined area for La Ceiba, and in pink for La Ensenada. Narrower colored bands show the temperature range inferred from pyroxene compositions alone in the assemblage space consistent with the mineralogy. The area around "Albitite" is the greenschist condition for the albitite/alteration of jadeitites from north of the Motagua fault. A facies grid for metabasalts that is a hybridization of Oh and Liou (1998) and Peacock (1993) is shown for reference; facies symbols are ZE: zeolite, PA: pumpellyite actinolite, GS: greenschist, AM: amphibolite, EpA: epidote amphibolite, EpB: epidote blueschist, LwsB: lawsonite blueschist, AmpEC: amphibole eclogite, ZoEC: zoisite eclogite, and LwsEC: lawsonite eclogite. Reactions are from Harlow (1994) plus pumpellyite calculations from GeoCalc (Berman et al., 1987, Berman, 1988, 1991). Reactions defined by an integer are (1) 4Lws + 2Anl = Ab + Pg + 2Czo + 8W; (2) 4Lws +2Jd = Ab + Pg + 2Czo + 6W; (3) 4Lws + Jd = Qtz + Pg + 2Czo; (4) 4Lws + Ab = 2Qtz + Pg + 2Czo + 6W; (5) 3Ab + 4 Pmp = 2 Jd + 6 Czo + Pg + 4 Di + 10 W. Ab: Albite, Anl: Analcime, Czo: Clinozoisite, Di: Diopside, Jd: Jadeite, Lws: Lawsonite, Ne: Nepheline, Pg: Paragonite, Pmp: Pumellyite, Qtz: Quartz, W: H_2O.**

Oberhänsli et al. (2007) used the method of pseudosections to calculate conditions for bulk compositions of jadeitite from Sorkhan, Iran and elsewhere, including an estimate for a sample north of the Motagua fault: R11 called Olmec-Blue containing jadeite, albite, paragonite, analcime, zoisite, titanite, and preiswerkite (Harlow, 1994). Their analysis yields T=~500ºC and P=~14kbar, at the high end of our T estimate and above our P estimate. However, this estimate is defined by the lack of omphacite and presence of zoisite, whereas jadeitites from north of the Motagua fault usually contain primary omphacite and late or alteration zoisite. The authors state that the presence of jadeite + omphacite yields *T*s below 400ºC in their calculations, more consistent with the results of Harlow (1994) and those presented here. Ultimately, their results are useful but may be difficult to apply to jadeitites North of the Motagua fault where bulk composition is strongly affected by alteration and phase assemblages must be deciphered for different stages of the rock history.

The jadeitite from Saltán is singular for samples that contain late-stage pumpellyite + grossular as well as nearly pure jadeite; however, the primary crystallization of the jadeite in these lavender-colored rocks provides little indication for initial conditions as inclusions are generally fluids and jadeite in contact with albite has rounded grain boundaries as if in reaction relationship. Omphacite is absent. Another sample from Saltán (MVE07B-19-6) contains albite and omphacite inclusions in jadeite and no pumpellyite or vesuvianite, more like other samples from the western end of the northern suite. Our conclusion is that the lavender samples represent both a different origin condition and composition (low Fe), and the alteration assemblage pumpellite + albite + grossular + zoisite/clinozoisite suggests T~350ºC at P 6-8kbar (e.g., Schiffman and Liou 1980), which is probably colder than jadeitite-albitite conditions found elsewhere North of the Motagua fault. Another distinctive aspect of these jadeitites is the late extensive enrichment in both Sr and Ba.

PT conditions South of the Motagua fault

Whereas the phase assemblages for the entire 200km span of jadeitite north of the Motagua fault (except Saltán) are remarkably consistent, those south of the Motagua fault clearly group into three distinct clusters based on geography. In jadeitites from the Carrizal Grande area, the presence of quartz inclusions in jadeite indicates P in the jadeite + quartz stability field. They are found together with lawsonite eclogites with maximum metamorphism estimated at P=20-26kbar, T=350-480°C and blueschist alteration from P≈14kbar and T≈400°C indicating a geotherm of ≈5°C/km, comparable to the coldest geotherms from subduction zones worldwide (Tsujimori et al., 2006a). Jadeitites at Carrizal Grande are consistent as a phase assemblage with the blueschist trajectory of this interpretation, but not well constrained. In this case, the results of Oberhänsli et al. (2007) may provide useful insight, as the assemblages of quartz-lawsonite-jadeite-omphacite-amphibole-paragonite have a narrow stability field from 350-425ºC and 11-16kbar (their Fig. 4A), although Carrizal Grande samples contain phengite rather than paragonite and thus have a different bulk composition.

Consequently, jadeitite formation is estimated as T<500ºC (those with lawsonite, <450ºC) and P=12-20kbar in the presence of lawsonite; without lawsonite T can only be estimated from coexisting omphacite-jadeite, which is discussed below. Jadeitites from La Ceiba also manifest quartz inclusions in jadeite but contain neither lawsonite nor zoisite/clinozoisite to further constrain the phase assemblage in PT. Compared to Carrizal Grande jadeitites, jadeite - omphacite pairs at La Ceiba suggest a somewhat lower maximum T of ~450ºC. That plus the lack of coexisting eclogite in the local mélange but presence of glaucophane blueschists argues for somewhat lower P of ~12-16?kbar. In the La Ensenada jadeitite the lack of quartz, intimate pumpellyite - jadeite textures, and a large omphacite-jadeite gap suggests maximum T=<300-350ºC at P>6kbar.

Mechanism of formation

Previous work on Guatemalan jadeitite (Harlow, 1994) and jadeitite in general (Sorensen et al., 2006; Harlow et al., 2007) has argued for crystallization from a hydrous fluid, derived from a subduction channel, in fractures in serpentinizing peridotite, presumably the hanging wall (the mantle wedge) of the channel. The fundamental arguments are 1) consistent association with serpentinite with some clear cases of contact (*e.g.*, Myanmar – see Harlow et al., 2007), 2) textural evidence for crystallization from a fluid including abundant fluid inclusions and unimpeded crystal growth into open space, 3) little evidence for metasomatic replacement of a protolith in terms of either pseudomorphic textures or relict phases from such a protolith, 4) evidence that high pressure hydrous fluids, such as those derived from the blueschist-to-eclogite transition are mostly saturated with respect to jadeite (Manning, 1998), 5) reaction zones between jadeitite and serpentinite that represent primary or secondary interactions involving a fluid (Sorensen et al., 2010; Harlow et al., 2007). This report updating jadeitite information from Guatemala reinforces these observations. Harlow et al. (2007) cite one case where metasomatic replacement has been documented – Punta Rasciassa in the Monviso serpentinite of the Western Alps, Italy (Compagnoni et al., 2007) and two cases in which jadeitite encapsulates eclogite blocks in a mélange – Kampos mélange, Syros, Cyclades, Greece (Bröcker and Keasling, 2006) and Borus mélange, Khakassia (Dobretsov, 1963). Among more than 100 jadeitite samples examined in this study only a few might be invoked to show metasomatic replacement, and these are most clearly limited to relict garnet: ZC20 and MVE06-17-2. Interestingly, both samples contain metamorphic garnets that are not likely from any eclogite or garnet amphibolite (metabasite) associated with the mélanges as the spessartine content exceeds that in the metabasites. Certainly there are ambiguous cases of jadeite nucleation around another mineral like zircon, uraninite and even albite, but the minerals are either totally exotic (uraninite) or found within the phase assemblages of jadeitite without clearly exotic compositions so metasomatism is not documented.

Pyroxene zoning, pyroxene pairs and P-T-t paths

The evaluation of the solvus in the jadeite – diopside – hedenbergite - aegirine clinopyroxene system by Green et al. (2007) has been applied to compositional data compiled on the pyroxenes in this study of jadeitite. Pressure has been uniformly set at 12kbar as a reasonable average for the pseudobinary evaluations along the (diopside + hedenbergite + aegirine) - jadeite joins, following the example of García-Casco et al. (2009). Several implications have been derived.

Firstly, only rare pairs give consistent T estimates, which is evident from Fig. 6. Omphacite consistently yields a higher T estimate than jadeite, typically by 100 to 150ºC. Whereas this could be interpreted as due to disequilibrium at low T and problems with the aegirine estimate, the consistency among many pairs from different samples and locations argues against this. Given the gentler slope of solvus for jadeite compositions and their dominance, we have used them for subsequent discussion.

The second implication is derived from the zoning of jadeite crystals with omphacite inclusions or overgrowths. The recently described jadeitites from Cuba (García Casco et al., 2009) have been interpreted with a considerably different sequence of conditions during growth than for others (Harlow et al., 2007). Cores of jadeite manifest oscillatory zoning of impure jadeite interpreted as forming at higher temperatures, ca. 640ºC, with a change to binary jadeite-omphacite crystallization (a more diopside-rich fluid) at ca. 570ºC on jadeite crystal rims. This observation led us to reexamine zoning in Guatemalan jadeite and jadeite-omphacite pairs. Jadeite-rich cores and jadeite-poor rims in most Guatemalan jadeitite are the reverse of those reported by García-Casco et al. (2009) and consistent with those previously reported (Harlow, 1994; Sorensen et al., 2006; Harlow et al., 2007). Indeed, many jadeitite samples, with few exceptions, crystallize with a jadeite-rich core (Jd_{100-95}) with an overgrowth extending to perhaps Jd_{85-80} followed by omphacite. These final jadeite compositions in equilibrium with omphacite yield T=500-580ºC based on the solvus of Green et al. (2007). Pure jadeite cores alone only demand a fluid that is saturated with respect to jadeite and presumably not saturated in other components or phases and thus cannot be used to assess T. However, in numerous samples omphacite inclusions in the interior of jadeite grains appear to be (nearly) in equilibrium with the adjacent jadeite. For these pairs, T is about

200-300ºC for P assumed to be 10-12kbar and should define roughly the initial growth conditions. Decrease in jadeite content with continued grain growth requires higher T, otherwise omphacite would form. Ultimately, jadeite grain compositions decrease to Jd_{80} followed by omphacite compositions that can, with continued crystallization along grain boundaries, evolve to diopside > jadeite and, in some cases, distinct diopside coexisting with albite. These trends suggest up-T crystallization plus increasing diopside-content of the fluid, in part contradictory to our previous interpretation (Harlow et al., 2007).

Zoning within jadeite crystals is commonly cryptic in interiors and rhythmic toward the rims. Cryptic zoning is puzzling but may combine aspects of fast crystallization and deformation as many cryptically zoned crystals have fuzzy optical extinction. Rhythmic zoning has been explained as the result of pulses of fluid entering open fractures in preexisting jadeitite that crystallizes more jadeite-rich compositions first with depletion leading to compositions higher in other components (Harlow, 1994; Sorensen et al., 2006).

Studies of jadeitites along with many other HP–LT rock P-T-t-x paths following a clockwise PT history argue that jadeitite formation should follow a down-P, down-T path during exhumation (e.g., Harlow et al., 2007; Tsujimori et al., 2006a; Sorensen et al., 2006; Harlow et al., 2003). The composition of coexisting jadeite-omphacite in the cores of jadeite crystals as compared to rims generally argue for either cold primary crystallization followed by hotter late crystallization or composition of jadeite controlled strictly by fluid composition with omphacite being in disequilibrium, perhaps encapsulated from a dismembered omphacite-bearing protolith. The lack of replacement textures (see below) and dissimilarity of omphacite compositions to any known mélange lithology make the second explanation less credible. Thus, we prefer the interpretation in which initial jadeitite crystallization is colder (ca. 300ºC) with late crystallization and omphacite veining as warmer (perhaps to 500ºC). This implies that the most jadeitite crystallizes in a chilled environment that later experiences warming while the crystallization simultaneously evolves toward more diopside (+ hedenbergite + aegirine) bulk composition. This would appear to be an improbable coincidence, but support for an alternate hypothesis is not compelling. Finally, there are a number of samples that show more than one generation of higher initial jadeite content growth followed by decreasing jadeite (e.g., MVE04-15-3 – La Ceiba: Fig. 7D; or JJE01-3-1 – Carrizal Grande Fig. 5N). Multiply zoned jadeite records a repeat of whatever sequence of events and processes responsible for zoning profiles in most jadeitites from Guatemala.

Consequently, crystallization of jadeitite probably should not be viewed as directly connected to some phase of the metamorphism of the subducted slab, such as eclogite or blueschist formation, because jadeitite most likely formed in the hanging wall, or a slice thereof, rather than in the slab. However, jadeite veins in some Lawsonite-eclogite from Carrizal Grande (Tsujimori et al., 2005, 2006a), suggest that at least a portion of jadeitite formation postdates that of eclogite and that either the jadeitite-forming fluids were active in portions of the subduction channel or eclogite had been incorporated into the serpentinizing mélange by the time of jadeitite formation. The interpreted progression of colder to warmer crystallization of jadeite unfortunately does not include any pressure information. It is unlikely that the process happens deeper than the transition from static mantle wedge to ductile where it is being dragged down with the plate, roughly at 70-80km depth (~23-26kbar; e.g., Grove et al., 2009.) So, it is not clear whether the trend tracks heating due to the exothermic serpentinization reactions (see Evans, 2004) plus aging of the contact or delamination of mantle wedge slabs via volume increase (from serpentinization) and increased traction or some other process. Cycling of this process might be explained by small scale wedge extrusion –decreasing P– with or without delamination of the overlying wedge into the subduction channel that puts colder slab and new fluids adjacent to the serpentinizing mantle. Resolution requires better control of P-T-t-x interpretation as well as modeling.

Differences between jadeitite from North and South of the Motagua fault

From the descriptions above, it is clear that jadeitite occurrences North and South of the Motagua fault vary in some very distinctive ways. The first to be considered is the tectonic context. South of the Motagua fault, eclogite and jadeitite are part of a single tectonic event (collision-exhumation) that spans eclogite crystallization from 144-132 (±~10; Sm-Nd) Ma and thermal closure (Ar-Ar) from 125-116Ma, whereas North of the Motagua fault there are clearly two events defined by mélange eclogite (131-126Ma; Sm-Nd), more or less equivalent to dates south of the Motagua fault, and thermal closure ages from 65 to 77Ma, equivalent to metamorphic ages (Ar-Ar of mica and amphibole in gneisses and Sm-Nd isochrons for eclogite enclaves, e.g., Martens et al., 2007a) from the Sierra de Las Minas, north of the mélange (Brueckner et al., 2009). Recent crystallization dates for jadeitite are limited but intriguing. U-Pb dating of zircon from a single jadeitite in the central zone north of the Motagua fault gives 95.1±3.6Ma (Yui et al., 2010) which was concluded to be a formation date on the basis of inclusions in the zircons. This age is certainly younger than the eclogite date but somewhat older than the Cretaceous event that metamorphosed the Sierra de Las Minas and

emplaced the Sierra de Santa Cruz ophiolite. A U-Pb date from a phengite jadeitite (MVE02-8-6) from south of the Motagua fault of 153.7±3.5Ma (Fu et al., 2010) was interpreted as a protolithic relic from the oceanic crust based on its being older than the eclogite ages. However, we have doubts about this interpretation: the zircon in this sample contain mineral and fluid inclusions inconsistent with an igneous origin, and being older is not a necessarily a criterion for being relict. Certainly, these dates raise a variety of interesting questions beyond the scope of this paper without more zircon dating, but it does appear that this difference between the jadeitite north and south of the Motagua fault is real. The presence or lack of albitization, albite-mica rocks, etc. may be related to both temporal and physicochemical differences in the formation events.

The next distinction is the vast areal extent of the northern jadeitite belt, more than 200km with at least three grouped areas compared to a very limited extent, ~11km, parallel to and south of the Motagua fault. All of the jadeitite north of the Motagua fault shares the extensive albitization overprint, whereas the narrow extent of jadeitite south of the Motagua fault can be readily distinguished among three fault slices by different phase assemblages and apparent P and/or T of crystallization. Moreover, quartz inclusions and veins in jadeite from two of the three occurrences south of the Motagua fault stands in contrast to the total lack of quartz in any jadeitite from north of the Motagua fault. So, clearly the different tectonic events have made a difference, but whether the lack of variability on the north side is due entirely to a possible Cretaceous overprint or to different formational events is not yet clear. If the zircon dating holds, the Cretaceous age is the crystallization date and the alteration is just part of the northern processing.

The lavender-colored jadeite in samples from Saltán, north of the Motagua fault, and La Ensenada, south of the Motagua fault, deserve special mention and attention. The jadeite in these samples has compositions among the most rich in jadeite component and lowest in iron. Likewise, coexisting omphacite (found so far only at La Ensenada), pumpellyite, and lawsonite (south only) suggest the lowest crystallization temperatures for jadeitite. The minimal iron in both pyroxene and clinochlore (La Ensenada) suggest some mechanism for keeping ferrous iron in solution during crystallization which could be related to some redox phenomenon such as that which leads to removal of iron in white bauxites during low-T diagenesis (Feenstra, 1996; see Lu et al., 2005), as well as low-T, in general, for the formation of these distinct jadeitite.

Finally, although this paper does not present rock compositions and geochemistry, an obvious difference from the mineralogy between the northern and southern jadeitite is the predominant mica. Jadeitite north of the Motagua fault predominantly features paragonite with very secondary abundance of phengite and phlogopite plus alteration preiswerkite. In contrast, paragonite (and preiswerkite) are absent in jadeitite south of the Motagua fault, whereas phengite is common to abundant. Interestingly, the late barium influx is common in all Guatemalan jadeitite occurrences by the presence of barian K-micas, cymrite, celsian, banalsite, and hyalophane. The chemically distinctive mineralogies are suspected to be attributed to the compositional characteristics of the sediments accompanying the subducted slab that sourced jadeitite-forming fluid. This would suggest a decoupling of potassium sourcing, probably from clays and continentally derived sediments, from barium, more likely coming from either oceanic seafloor sediments or carbonates. These and other geochemical issues are being taken up elsewhere.

CONCLUSION

The distribution of jadeitite in Guatemala is now known to extend for more than 200km in serpentinite mélange strung out north of the Motagua fault and in three newly described mélange slices south of the fault. All of the jadeitite from north of the Motagua fault is characterized by jadeite containing inclusions or veins of albite + omphacite ± anaclime ± paragonite ± nepheline with extensive albitization. Jadeitite from the three known sources south of the Motagua fault are distinctive by their mineralogy and associated mélange lithologies: Carrizal Grande jadeitite features jadeite with inclusions of quartz + omphacite + phengite, minor veining of quartz or albite, a substantial proportion of samples containing lawsonite, and associated lawsonite - eclogite; La Ceiba has jadeitite similar to Carrizal Grande minus any lawsonite and omphacite bearing gneisses instead of eclogite; and La Ensenada has distinctive light-colored pumpellyite - jadeitite with veins of grossular plus albite and contacts with clinochlore rock in a mélange containing lawsonite - glaucophane blueschist. All evidence points to jadeitite formation from primary crystallization of jadeite and other phases from hydrous fluid liberated from the subducted slab and introduced into peridotite/serpentinite of the overriding mantle wedge. The extent of jadeitite in Guatemala is second only to Myanmar and the complexity of the tectonic context is noteworthy: Two collisions are recorded in the HP–LT blocks from the northern and southern serpentinite mélanges, one Neocomian and the other Maastrichtian, and it appears jadeitite formed in both events.

ACKNOWLEDGMENTS

We want to thank Carlos Gonzales for field assistance and Eric Sahm and Jamie Newman for analytical and sample processing

assistance and John Cleary for sharing geological observations from mapping observations on the jade deposits near Carrizal Grande. This work was funded by EAR0309320 to GEH, and EAR0309116 to VBS. This project is part of IGCP Project 546 on Subduction Zones of the Caribbean. We appreciate constructive reviews by Walter Maresch and Tatsuki Tsujimori.

REFERENCES

Alvarado, G.E., Dengo, C., Martens, U., Bundschuh, J., Aguilar, T., Bonis, S.B., 2007. Stratigraphy and geologic history. In: Bundschuh, J., Alvarado, G.E. (eds.). Central America: Geology, Resources, and Hazards. London, Taylor and Francis Group, 345-483.

Berman, R.G., 1988. Internally-consistent thermodynamic data for minerals in the system K_2O-Na_2O-CaO-MgO-FeO-Fe_2O_3-Al_2O_3-SiO_2-TiO_2-H_2O-CO_2-O. Journal of Petrology, 29, 445-522.

Berman, R.G., 1991. Thermobarometry using multi-equilibrium calculations: a new technique, with petrological applications. Canadian Mineralogist, 29, 328-344.

Berman, R.G., Brown, T.H., Perkins, E.H., 1987. GE0-CALC Software for the calculation and display of pressure-temperature-composition phase diagrams. Vancouver, University of British Columbia.

Bertrand, J., Vuagnat, M., 1976. Etude pétrographique de diverses ultrabasites ophiolitiques du Guatémala et de leurs inclusions. Bulletin Suisse de Minéralogie et Pétrologie, 56, 527-540.

Bertrand, J., Vuagnat, M., 1980. Inclusions in the serpentinite melange of the Motagua Fault Zone, Guatemala. Société de Physique et D'Histoire Naturelle de Genève, Archives des Sciences, 33, 321-336.

Bröcker, M., Keasling, A., 2006. Ionprobe U-Pb zircon ages from the high-pressure/low-temperature melange of Syros, Greece: age diversity and the importance of pre-Eocene subduction. Journal of Metamorphic Geology, 24, 615-631.

Brueckner, H.K., Avé Lallemant, H.G., Sisson, V.B., Harlow, G.E., Hemming, S.R., Roden-Tice, M.K., Sorensen, S.S., Tsujimori, T., Francis, A.H., Gehrels, G.E., Blythe, A.E., 2009. Metamorphic reworking of a high-pressure-low temperature serpentinite-matrix mélange belt north of the Motagua fault, Guatemala: A revised record of Neocomian and Maastrichtian collisions. Earth and Planetary Science Letters, 284, 228-235.

Brueckner, H.K., Hemming, S., Sorensen, S., Harlow, G.E., 2005. Synchronous Sm-Nd mineral ages from HP Terranes on both sides of the Motagua Fault of Guatemala: convergent suture and strike slip fault? Eos Transactions American Geophysical Union, Fall Meeting Supplement, 86(52), Abstract T23D-04.

Carpenter, M.A., 1979. Omphacites from Greece, Turkey, and Guatemala: Composition limits of cation ordering. American Mineralogist, 64, 102-108.

Carpenter, M.A., 1981. Time-temperature-transformation (TTT) analysis of cation disordering in omphacite. Contributions to Mineralogy and Petrology, 78, 433-440.

Chiari, M., Dumitrica, P., Marroni, M., Padolfi, L., Principi, G., 2006. Radiolarian biostratigraphic evidence for a Late Jurassic age of the El Tambor Group Ophiolites (Guatemala). Ofioliti, 31(2), 173-182.

Compagnoni, R., Rolfo, R., Manavella, F., Salusso, F., 2007. Jadeitite in the Monviso meta-ophiolite, Piemonte Zone, Italian western Alps. Periodico di Mineralogia, 76, 79-89.

Dobretsov, N.L., 1963. Mineralogy, petrography and genesis of ultrabasic rocks, jadeitites, and albitites from the Borus Mountain Range (the West Sayan). Academia Scientifica USSR (Siberian Branch), Proceedings of the Institute of Geology and Geophysics, 15, 242-316.

Donnelly, T.W., Horne, G.S., Finch, R.C. López-Ramos, E., 1990. Northern Central America; The Maya and Chortís Blocks. In: Case, J.E., Dengo, G., (eds.). The Geology of North America, The Caribbean Region. Boulder CO, Geological Society of America, H, 37-76.

Evans, B., 2004. The serpentinite multisystem revisited: Chrysotile is metastable. International Geology Review, 46, 479-506.

Feenstra, A., 1996. An EMP and TEM-AEM study of margarite, muscovite and paragonite in polymetamorphic metabauxites of Naxos (Cyclades, Greece) and the implications of fine-scale mica interlayering and multiple mica generations. Journal of Petrology, 37, 201-233.

Finger, L.W. 1972. The uncertainty in the calculated ferric iron content of a microprobe analysis. Carnegie Institution of Washington, 71(Yearbook), 600-603.

Foshag, W.F., 1957. Mineralogical studies on Guatemalan jade. Smithsonian Miscellaneous Collections, 135(5), 60pp.

Foshag, W.F., Leslie, R., 1955. Jadeite from Manzanal, Guatemala. American Antiquity, 21, 81-83.

Francis, A.H., 2005. Deformation history of the Maya and Chortís Blocks: Insight to the Evolution of the Motagua Fault Zone, Guatemala. Doctoral Thesis. Houston, Rice University, 149pp.

Francis, A.H., Avé Lallemant, H.G., Sisson, V.B., Harlow, G.E., Donnelly, T.W., Chiquin, M., Roden-tice, M.K., Hemming, S.R., Brueckner, H.K., in preparation. Interaction of the North American and Caribbean plates in Guatemala: Part 1. Deformation history and consequences for the exhumation of HP/LT metamorphic rocks. For Geological Society of America Bulletin.

Fu, B. Valley, J.W., Kita, N.T., Spicuzza, M.J., Paton, C., Tsujimori, T., Bröcker, M., Harlow, G.E., 2010. Origin of zircons in jadeitite. Contributions to Mineralogy and Petrology, 159, 769-780. doi: 10.1007/s00410-009-0453-y

García-Casco, A., Rodríguez Vega, A., Cárdenas Párraga, J., Iturralde-Vinent, M.A., Lázaro, C., Blanco Quintero, I., Rojas Agramonte, Y., Kröner, A., Núñez Cambra, K., Millán, G., Torres-Roldán, R.L., Carrasquilla, S., 2009. A new jadeitite jade locality (Sierra del Convento, Cuba): first report and some petrological and archeological implications. Contributions to Mineralogy and Petrology, 158, 1-16. doi: 10.1007/s00410-008-0367-0

Green, E.C.R., Holland, T.J.B., Powell, R., 2007. An order-disorder model for omphacitic pyroxenes in the system jadeite-diopside-hedenbergite-acmite, with applications to eclogite rocks. American Mineralogist, 92, 1181-1189.

Grove, T.L., Till, C.B. Lev, E., Chatterjee, N., Médard, E., 2009. Kinematic variables and water transport control the formation and location of arc volcanoes. Nature, 459, 694-697.

Hammond, N., Aspinall, A., Feather, S., Hazelden, J., Gazard, T., Agrell, S., 1979. Maya Jade: Source location and analysis. In: Earle, T.K., Ericson, J.E., (eds.). Exchange Systems in Prehistory. New York, Academic Press, 3(Chapter), 35-67.

Harlow, G.E., 1994. Jadeitites, albitites and related rocks from the Motagua Fault Zone, Guatemala. Journal of Metamorphic Geology, 12, 49-68.

Harlow, G.E., 1995. Crystal chemistry of barian enrichment in micas from metasomatized inclusions in serpentinite, Motagua Valley, Guatemala. European Journal of Mineralogy, 7, 775-789.

Harlow, G.E., Brueckner, H., Sorensen, S.S., 2010. Serpentinites of the Motagua fault zone mélanges, Guatemala: An assessment. Annual Meeting, Geological Society of America, Abstracts with Programs, 42(5), Avaiable Online: http://a-c-s.confex.com/crops/2010am/webprogram/Paper181532

Harlow, G.E., Donnelly, T.W., 1989. Unusual metabasites from jadeitite-bearing serpentinite melange, Motagua Valley, Guatemala. Eos, 70 (Abstract), 505.

Harlow, G.E., Hemming, S.R., Avé Lallemant, H.G., Sisson, V.B., Sorensen, S.S., 2004a. Two high-pressure–low-temperature serpentine-matrix mélange belts, Motagua fault zone, Guatemala: A record of Aptian and Maastrichtian collisions. Geology, 32, 17-20.

Harlow, G.E., Murphy, A.R., Hozjan, D.J., de Mille, C.N., Levinson, A.A., 2006a. Pre-Columbian jadeite axes from Antigua, West Indies: Description and possible sources. Canadian Mineralogist, 44, 305-321.

Harlow, G.E., Olds, E.P., 1987. Observations on terrestrial ureyite and ureyitic pyroxene. American Mineralogist, 72, 126-136.

Harlow, G.E., Price, N.A., Tsujimori, T., 2006b. Serpentinites of the Motagua fault zone, Guatemala: A mineralogical assessment. Kobe (Japan), 19th General Meeting of the International Mineralogical Association Program & Abstracts, 223, 19-17.

Harlow, G.E., Quinn, E.P., Rossman, G.R., Rohtert, W.R., 2004b. Blue omphacite from Guatemala. Gem News International section – Gems and Gemology, 40, 68-70.

Harlow, G.E., Rossman, G.R., Matsubara, S., Miyajima, H., 2003. Blue omphacite in jadeitites from Guatemala and Japan. Seattle (Washington), 2003 Geological Society of America, Abstracts with Programs, 35(6), 620 (CD-ROM 254-1).

Harlow, G.E., Sorensen, S.S., Sisson, V.B., 2007. Jade. In: Groat, L.A. (ed.). The Geology of Gem Deposits. Quebec, Mineralogical Association of Canada, Short Course Handbook Series, 37, 207-254.

Lu, P.J., Yao, N., So, J.F., Harlow, G.E., Lu, J., Wang, G., Chaikin, P.M., 2005. Earliest use of corundum and diamond in prehistoric China. Archaeometry, 47, 1-12.

Manning, Craig E., 1998. Fluid composition at the blueschist-eclogite transition in the model system Na_2O-MgO-Al_2O_3-SiO_2-H_2O-HCl. Schweizerische Mineralogische und Petrographische Mitteilungen, 78(2), 225-242.

Martens, U., Ortega-Obregón, C., Estrada, J., Valle, M., 2007a. Metamorphism and metamorphic rocks. In: Bundschuh, J., Alvarado, G.E. (eds.). Central America: Geology, Resources, and Hazards. London, Taylor and Francis Group, 485-522.

Martens, U., Mattinson, C.G., Wooden, J., Liou, J.G., 2007b. Protolith and metamorphic ages of gneiss hosting eclogite in the Chuacús complex, Central Guatemala. Eos Transactions of the Amererican Geophysical Union, Joint Assemembly, Supplemet Abstract, 88(23), U53A-08McBirney, A.R., 1963. Geology of a part of the Central Guatemalan cordillera. University of California Publications in Geological Sciences, 38, 177-242.

McBirney, A.R., Aoki, K.-I., Bass, M., 1967. Eclogites and jadeite from the Motagua fault zone, Guatemala. American Mineralogist, 52, 908-918.

Nassau, K., Shigley, J.E., 1987. A study of the General Electric synthetic jadeite. Gems & Gemology, 23(1), 27-35.

Nyunt, T.T., Theye, T., Massonne, H.-J., 2009. Na-rich vesuvianite in jadeitite of the Tawmaw jade district, northern Myanmar. Periodico di Mineralogia, 78(3), 5-18.

Oberhänsli, R., Bousquet, R., Moinzadeh, H., Moazzen M., Arvin, M., 2007. The field of stability of blue jadeite: A new occurrence of jadeitite from Sorkhan, Iran, as a case study. The Canadian Mineralogist, 45, 1705-1713.

Oh, C.W., Liou, J.G., 1998. A petrogenetic grid for eclogite and related facies under high-pressure metamorphism. Island Arc, 7, 36-51.

Ortega-Gutiérrez, F., Solari, L.A., Solé, J., Martens, U., Gómez-Tuena, A., Morán-Ical, S., Reyes-Salas, M., Ortega-Obregón, C., 2004. Polyphase, high-temperature eclogite-facies metamorphism in the Chaucús complex, central Guatemala: Petrology geochronology and tectonic implications. International Geology Review, 46(5), 445-470.

Ouyang, Q., 2001. Characteristics of violet jadeite jade and its coloration mechanism. Baoshi He Baoshixue Zazhi, 3(1), 1-6.

Peacock, S.M., 1993. The importance of blueschist → eclogite dehydration reactions in subducting oceanic crust. Geological Society of America Bulletin, 105, 684-694.

Pouchou, J.L., Pichoir, F., 1991. Quantitative Analysis of Homogenous or Stratified Microvolumes Applying the Model "PAP". In: Heinrich, K.F.K., Newbury, D.E. (eds.). Electron Probe Quantitation. New York, Plenum Press, 31-75.

Schiffman, P., Liou, L., 1980. Synthesis and Stability Relations of Mg-Al Pumpellyite, $Ca_4Al_5MgSi_6O_{21}(OH)_7$. Journal of Petrology, 21, 441-474.

Seitz, R., Harlow, G.E., Sisson, V.B., Taube, K.E., 2001. "Olmec Blue" and Formative jade sources: new discoveries in Guatemala. Antiquity, 87, 687-688.

Silva, Z.C.G. da, 1967. Studies on jadeites and albitites from Guatemala. Master of Arts Thesis. Houston, Rice University, 21pp.

Silva, Z.C.G. da, 1970. Origin of albitites from eastern Guatemala. Boletim dos Serviços de Geologia e Minas (Brazil), 22, 23-32.

Sorensen, S., Harlow, G.E., Rumble, D., 2006. The origin of jadeitite-forming subduction zone fluids: CL-guided SIMS oxygen isotope and trace element evidence. American Mineralogist. 91, 979-996.

Sorensen, S.S., Sisson, V.B., Harlow, G.E., Avé Lallemant, H.G., 2005. Geochemistry of a jadeitite-serpentinite contact, Guatemala. Salt Lake City (Utah), Geological Society of America Annual Meeting, Abstracts with Program, 37(5), 125.

Sorensen, S.S., Sisson, V.B., Harlow, G.E., Avé Lallemant, H.G., 2010. Element transport and residence sites during subduction zone metasomatism: Evidence from a jadeitite-serpentinite contact, Guatemala. International Geology Review.

Taube, K.A., Sisson, V.B., Seitz, R., Harlow, G.E., 2004. The sourcing of Mesoamerican jade: Expanded geological reconnaissance in the Motagua Region, Guatemala. In: Taube, K.A. (ed.). Olmec Art and Dumbarton Oaks. Pre-Columbian Art at Dumbarton Oaks, Dumbarton Oaks, 2, Washington, 203-228.

Tsujimori, T., Liou, J.G., Coleman, R.G., 2004a. Comparison of two contrasting eclogites from the Motagua fault zone, Guatemala: Southern lawsonite eclogite versus northern zoisite eclogite. Denver (Colorado), Geological Society of America Annual Meeting Abstracts and Program, 36(5), 1-36.

Tsujimori, T., Liou, J.G., Coleman, R.G., 2004b. A pictorial introduction to coarse-grained symplectites in low-temperature jadeitite from Guatemala. Journal of Geological Society of Japan, 110, XVII-XVIII.

Tsujimori, T., Liou, J.G., Coleman, R.G., 2005. Coexisting retrograde jadeite and omphacite in a jadeite-bearing lawsonite eclogite from the Motagua Fault Zone, Guatemala. American Mineralogist, 90, 836-842.

Tsujimori, T., Sisson, V.B., Liou, J.G., Harlow, G.E., Sorensen, S.S., 2006a. Petrologic characterization of Guatemala lawsonite eclogite: Eclogitization of subducted oceanic crust in a cold subduction zone, In: Hacker, B.R., McClelland, W.C., Liou, J.G. (eds.). Ultrahigh pressure metamorphism: Deep continental subduction. Geological Society of America, 403 (Special Publications), 147-168.

Tsujimori, T., Sisson, V.B., Liou, J.G., Harlow, G.E., Sorensen, S.S, 2006b. Very-low-temperature record of the subduction process: A review of worldwide lawsonite eclogites. Lithos, 92(3-4), 609-624.

van den Boom, G., 1972. Petrofazielle Gliedrung des metamorphen Grudgebirges in der Sierra de Chuacús, Guatemala. Beihefte Geologisches Jahrbuch, 122, 5-49.

Yui, T-F., Maki, K., Usuki, T., Lan, C-Y., Martens, U., Wu, C-M., Wu, T-W., Liou, J.G., 2010. Genesis of Guatemala jadeitite and related fluid characteristics: Insight from zircon. Chemical Geology, 270, 45-55.

Manuscript received January 2011;
revision accepted May 2011;
published Online June 2011.

ELECTRONIC APPENDIX

TABLE I | **Rocks studied and abbreviations for mineral names**

	Locality Name	N.Lat.	W.Long.	Description	Jd	Omp	Ab	Anl	Wm	Amp	Grt	Pmp	Zo	Lws	Apt	Rt	Ttn	Zrn	Qtz	Chl	Other
NORTH of Motagua fault. Western Region																					
MVE07B-19-1	Q nr. Saltán	14.884º	90.595º	Lavender jadeitite	x		x		Ms		Grs	x	Sr-Zo				x	x			Kfs
MVE07B-19-4	Q nr. Saltán	14.884º	90.595º	Lavender jadeitite	x		x		Ms, Ph		Grs	x	Sr-Zo				x				Ves, Kfs?
MVE07B-19-6	Q nr. Saltán	14.884º	90.595º	Jadeite metabasite?	x	x	x		Ba-Ph				Czo			?	x			x	
MVE07B-X-2	nr. Saltán	14.884º ?	90.595º ?	Pale-green jadeitite	x	x	x	x													
MVE06-X-1	Pachalum	14.884º ?	90.595º ?	White jadeitite	x	x	x		Prs	Mtar							x	x			Ne, Gph
MVE07-1	El Chol?	14.892º ?	90.549º ?	White jadeitite	x	x	x										x	x			
MVE07-5	El Chol?	14.892º ?	90.549º ?	Yellowish-green jadeitite	x	x	x		Prs				Al				x				
MVE06-4-3	Granados	14.892º	90.549º	White albitized jadeitite		?	x	?	x	Tr							x				
MVE04-44-1	Q. Los Pescaditos	14.852º	90.444º	White jadeitite w/ emerald green zones	x	x	x	x	Pg, Ph, Prs				Czo								Bnl, Ne
MVE04-44-2	Q. Los Pescaditos	14.852º	90.444º	White jadeitite	x	x	x	x	Pg				Czo				x				Ne
MVE04-44-4	Q. Los Pescaditos	14.852º	90.444º	White jadeitite	x	x	x	x	Pg,Prs				Czo				x				Bnl, Ne
NORTH of Motagua fault. Central Region																					
MVE04-30-1	CA 7, Morazán	14.904º	90.169º	White albitized jadeitite	x	x	x	?	Ba-Ph								x			x	Kfs, Cln?
MVE06-13-4	Río Comaja	14.944º	90.056º	Grayish jadeitite	x	x	x	x													
R-18	Río Comaja	14.944º	90.056º	Dark blue-green omphacitite	x	x	x		Ph	?	Sps-Grs-Alm		Al				x			x	Py, Cpy
MVE02-39-5	Pica pica	14.931º	89.961º	Greenish white jadeitite	x	x	x	x	Pg				x			x	x	x			
MVE02-39-6	Pica pica	14.931º	89.961º	Greenish white jadeitite	x	x	x	x	Phl, Ph				Czo								Ne?
MVE07-2	Pica pica	14.931º	89.961º	White jadeitite	x		x	x	Ms, Ph				Zo, Czo				x				Kfs
MVE03-81-3	El Mapache	15.008º	89.863º	Med. green jadeitite	x	x	x	x	Prs	Mtar			x				x				Unk
MVE03-82-3	El Mapache	15.007º	89.864º	Med. green jadeitite w/ veins	x	x	x	x	Pg	Mtar											
MVE04-24-4	Above Dos Ríos	15.020º	89.802º	White jadeitite w/veins	x	x	x	x	Pg	Mtar			Zo								
MVE04-25-6	Piedra Parada	15.012º	89.811º	Green omphacitite		x	x		Phl								x				

TABLE I | **Continued**

	Locality Name	N.Lat.	W.Long.	Description	Jd	Omp	Ab	Anl	Wm	Amp	Grt	Pmp	Zo	Lws	Apt	Rt	Ttn	Zrn	Qtz	Chl	Other
MVE07-4	Los Vados, El Jute	14.977°	83.835°	Dark green omphacitite	x	x	x								x						
MVE07-7	Estancia de La Virgen	14.941°	89.885°	Omp-Jadeitite	x	x	x	x		Mtar							x	x			
ZC20	NW Manzanal	14.939°	89.871°	Med. green jadeitite	x	x				Ftar	Alm		Czo, Al				x				
MVJ84-3-4	Manzanal	14.942°	89.852°	White jadeitite	x		x	x													
MVE04-26-2	W Río Uyus	14.941°	89.836°	White-green jadeitite	x	x	x	x	Pg				x				x				
NHMLAC 20368	Guat. I	15°	89.8°	Green omphacitite	x	x	x		Pg, Phl								x	x		x	K-Bafs
MVJ87-8-1	Guat. I	15°	89.8°	Green Omphacitite	x	x	x	x	Ph, Pg, Phl				x		x	x	x				Kfs
MVJ87-8-2	Guat. I	15°	89.8°	Light blue-green jadeitite	x																
R-11	Guat. I	15°	89.8°	"Olmec Blue" jadeitite	x		x	x	Pg, Prs				x		x		x				
RSJ00-2	El Ciprés	15.073°	89.796°	Light green jadeitite	x	x	x		Prs?								x				
RSJ00-3	El Ciprés	15.073°	89.796°	Med. Blue-green jadeitite	x	x	x		Pg		Grs						x	x			
RSJ00-6	El Ciprés	15.073°	89.796°	Med. green jadeitite	x	x			Phl, Pg, Prs	Mtar			Czo				x				
RSJ00-7	El Ciprés	15.073°	89.796°	Med. green jadeitite	x	x	x										x	x			
RSJ01-1	El Ciprés	15.073°	89.796°	Pale green jadeitite																	
MVJ84-51-3	N. of Q. Escorpión	14.99°	89.787°	White-green jadeitite vein	x	x	x		Pg	Mtar			x				x				
RSJ01-8	nr Río La Palmilla	14.99°	89.787°	Pale green jadeitite w/ emerald green zones																	
MVJ84-9C-2	Río La Palmilla	14.99°	89.787°	Greenish white jadeitite	x	x	x	x	Pg, Prs	Mtar			Zo				x				
MVJ84-12-2	Río La Palmilla	14.99°	89.787°		x	x	x										x				
MVJ84-44-2	Río La Palmilla	14.99°	89.787°	Green omphacitite		x	x			Ftar					x		x				Cpy
MVE07-10	Río La Palmilla	14.99°	89.787°	Greenish white jadeitite	x	x	x	x													
MVJ84-29-2	Usumatlán	14.962°	89.762°	Bluish gray jadeitite	x	x	x		Pg, Phl	Mtar							x	x			Gph
MVE07B-3-1	Cerro Colorado	14.965°	89.759°	Green micaceous jadeitite	x	x	x		Phl, Ph, Pg				Czo					x			Hm, Br

TABLE I | **Continued**

	Locality Name	N.Lat.	W.Long.	Description	Jd	Omp	Ab	Anl	Wm	Amp	Grt	Pmp	Zo	Lws	Apt	Rt	Ttn	Zrn	Qtz	Chl	Other
MVE07B-3-2	Cerro Colorado	14.965º	89.759º	Light green jadeitite w/ red spots	x	x	x	x	Ph				Czo					x			Hm, Br
MVE07-8	Río Teculután	15.044º	89.748º	Dark green omphacitite	x	x	x			Ftar							x				
MVE02-2-5	Panaluya-Río Hondo	15.052º	89.59º	Green white jadeitite	x	x	x	x	Pg	Mtar					x		x	x			Bnl
MVE02-4-3	Panaluya-Río Hondo	15.032º	89.621º	Greenish white jadeitite	x	x	x	x	Pg, Bio				x								
MVE07-3	Río Hondo	15.052º	89.59º	Light green jadeitite	x	x							Czo				?	x			Bnl
NORTH of Motagua fault. Eastern Region																					
MVR07-25C	Rosario	16.182º	88.861º	Jadeitite-omphacitite	x	x	x	x	Ph, Pg								x	x	?		Gdf
MVR07-23C	Aldea Las Cruces	15.532º	88.829º	Med. green jadeitite	x	x	x	x	Pg, Ms, Phl				Czo-Zo				x				
MVR07-23D	Aldea Las Cruces	15.532º	88.829º	Med. green jadeitite	x	x	x	x	Ph, Pg								x	x			
MVR07-24C	Rosario	15.541º	88.829º	Light green jadeitite	x	x	x	x	Pg, Ph, Phl												
SOUTH of Motagua fault. Carrizal Grande																					
JJE01-3-1	S. Q. El Silencio	14.778º	89.893º	Dark-green Lws-jadeitite	x	x	x	x	Ph, Bio					x		x	x	x	x		
JJE01-3-2	S. Q. El Silencio	14.778º	89.893º	Med. green jadeitite	x	x	x	x	Ph, Bio								x	x	x	x	
JJE01-3-4	S. Q. El Silencio	14.778º	89.893º	Med. green jadeitite	x	x			Ph	Gln						x	x	x	?		
MVE02-8-5	Q. El Silencio	14.779º	89.888º	Light green Ph-jadeitite	x	x			Ph							x	x	x	x		
MVE02-8-6	Q. El Silencio	14.779º	89.888º	Light green Ph-jadeitite	x	x	x		Ph				Al			x	x	x	x		Mon
MVE07-9	Carrizal Grande	14.771º	89.886º	Light green jadeitite	x	x			Ph				x					x	x		
RSJ00-4	Q. del Mico	14.770º	89.882º	"Olmec-Blue" jadeitite	x	x	x		Ph				Czo, Al			x	x	x			Mon
MVE06-17-2	Q. del Mico	14.770º	89.882º	Grt jadeitite	x	x			Ph	Gln?	Alm		Czo	x		x	x	x	x		Gph
MVE03-80-1	Q. del Mico	14.772º	89.878º	Drk-green omphacitite		x, Di	x		Ph						x	x	x	x	?	x	Sr-Cc
MVE04-14-6	Q. Seca	14.768º	89.874º	Med. green jadeitite	x	x	x	x	Ph								x	x	x		Cym,
KT02-3b	Q. Seca	14.77º	89.873º	Blue to blue-green jadeitite	x	x							Al				x	x			Mon

TABLE I | **Continued**

	Locality Name	N.Lat.	W.Long.	Description	Jd	Omp	Ab	Anl	Wm	Amp	Grt	Pmp	Zo	Lws	Apt	Rt	Ttn	Zrn	Qtz	Chl	Other
RSJ01-X-1	Q. Seca	14.77º	89.873º	Green & blue-green omphacitite		x											x				
VM02-1	Q. Seca	14.77º	89.873º	Blue-green jadeititew/ blue vein	x	x											x				
MVE02-15-5	Q. Seca	14.77º	89.873º	Lws-omphacitite		x							x	x		x	x	x		x	Ba-Kfs
MVE02-15-6	Q. Seca	14.77º	89.873º	Dark green omphacitite	x	x	x		Ph								x	x	x		Kfs
MVE02-15-10	Q. Seca	14.77º	89.873º	Dark gray jadeitite	x	x, Di	x		Ph	Act			?		x		x	x	x		
MVE02-14-5	Q. del Mico	14.776º	89.868º	Chromian omphacite-glaucophane rock		x	x			Gln, Act											
JJE01-6-1	Río La Puerta	14.777º	89.863º	Dark-green Ph-Lws-jadeitite-omphacitite	x	x			Ph				?	x		x	x	x			
JJE01-6-2	Río La Puerta	14.777º	89.863º	Pheng-Omphacitite		x			Ph				x,al		x	x	x		x	x	Cc?
RSJ00-1	Río Jalapa	14.844	89.821	Speckled Olmec-blue	x	x	x		Ph								x				
JJE01-7-5	Río El Tambor	14.85º	89.815º	Nephrite / Diopsidite		Di				Tr	Grs		Al?								Cm, clay
JJE01-X-3	Río El Tambor	14.85º	89.815º	Med green Lws-jadeitite	x	x	x	x	Ba-Ph	Gln				x	x	x	x	x	x		
SOUTH of Motagua fault. La Ceiba																					
MVE03-77-1	La Ceiba	14.772º	89.828º	Dark green jadeite omphacitite	x	x	x		Ph				Al				x		x	x	
MVE03-77-3	La Ceiba	14.772º	89.828º	Dark green jadeite-omphacitite	x	x	x		Ph								x	x		x	Cln, Kfs
MVE03-77-4	La Ceiba	14.772º	89.828º	Dark green jadeite-omphacitite	x	x		x	Bio				Al		x				x		Cym, Hyl, Pect
MVE03-77-5-1	La Ceiba	14.772º	89.828º	Qtz jadeitite	x	x	x		Ph	Act							x		x		
MVE04-15-3	La Ceiba	14.771º	89.826º	Grn-Mauve jadeitite	x	x	x						REE-Czo		x		x	x	x		Cym, Uran
MVE02-17-5	La Ceiba	14.771º	89.826º	Med. Green jadeitite	x	x		x									x	x	x		Cym, Ves
SOUTH of Motagua fault. La Ensenada																					
MVE03-76-3a	Q. La Peña	14.822º	89.815º	brown prt/"Lila" jadeitite		x	x					x					x	x		x	
MVE03-76-3b	Q. La Peña	14.822º	89.815º	Lavender prt/"Lila" jadeitite	x	x	x		Ba-Ms		Grs	x	Zo?				x	x		x	Cln
MVE03-76-5	Q. La Peña	14.822º	89.815º	"Lila" jadeitite	x	x	x				Grs	x			x		x				
108353a	Q. La Peña	14.822º	89.815º	"Rainbow" jadeitite	x	x	x					x			x	x	x	x		x	

DOI: 10.1344/105.000001694

TABLE I | **Continued**

	Locality Name	N.Lat.	W.Long.	Description	Jd	Omp	Ab	Anl	Wm	Amp	Grt	Pmp	Zo	Lws	Apt	Rt	Ttn	Zrn	Qtz	Chl	Other
108353b	Q. La Peña	14.822º	89.815º	"Rainbow" jadeitite	x	x	x					x				x	x				
108354	Q. La Peña	14.822º	89.815º	"Rainbow" jadeitite	x	x						x					x				
108355	Q. La Peña	14.822º	89.815º	Pale green jadeitite	x		x		Ba-Ph			x					x				
MVE04-20-1	Q. La Peña	14.824º	89.814º	Mauve/orange jadeitite	x	x	x		Phl		Grs	x			x		x				
MVE04-20-3	Q. La Peña	14.824º	89.814º	White-Blue jadeitite	x		x		Ph		Grs	x	?			x	x	x			
MVE04-21-7	E of San Diego Rd	14.837º	89.79º	Wh-Or-Grn "Rainbow" jadeitite	x	x,Di	x				Grs						x		x		

JJE: Jalapa (southern) samples, MVJ: (northern) Motagua samples, RSJ: Russell Seitz jadeitite sample, R: Ridinger, Jade S.A.; Locality Guat 1 represents samples acquired from jade companies without specific location other than the central area north of the Motagua fault.

* The nomenclature of amphiboles is in transition, so we have chosen to explicitly distinguish ferro-taramite (new) from magnesiotaramite (old; actually alumino-magnesiotaramite to become taramite).

Ab: Albite, Act: Actinolite, Al: Allanite, Alm: Almandine, Amp: Amphibole, Anl: Analcime, Apt: Apatite, Bio: Biotite, Bnl: Banalsite, Cc: Chalcosite: Chl: Chlorite, Cln: Celsian, Cm: Corumdum, Cpy: Calcopyrite, Cym: Cymrite, Czo: Clinozoisite, Di: Diopside, Gln: Glaucophane, Gph: Graphite, Grt: Garnet, Grs: Grossular, Hm: Hematite, Hyl: Hyalophane, Jd: Jadeite, K-Bafs: K-Ba felspar, Kfs: K-felspar, Lws: Lawsonite, Mon: Monazite, Ms: Muscovite, Mtar: Magnesiotaramite, Ne: Nepheline, Omp: Omphacite, Pg: Paragonite, Ph: Phengite, Phl: Phlogopite, Pmp: Pumpellyite, Prs: Preiswerkite, Py: Pyrite, Qtz: Quartz, Rt: Rutile, Sps: Spessartine, Tr: Tremolite, Ttn: Titanite, Unk: Unknown, Uran: Uraninite, Ver: Vermiculite, Ves: Vesuvianite, W: H_2O, Wm: white mica, Zeo: Zeolite, Zo: Zoisite, Zrn: Zircon. –Suspected but unsubstantiated mineral due to inadequate data.